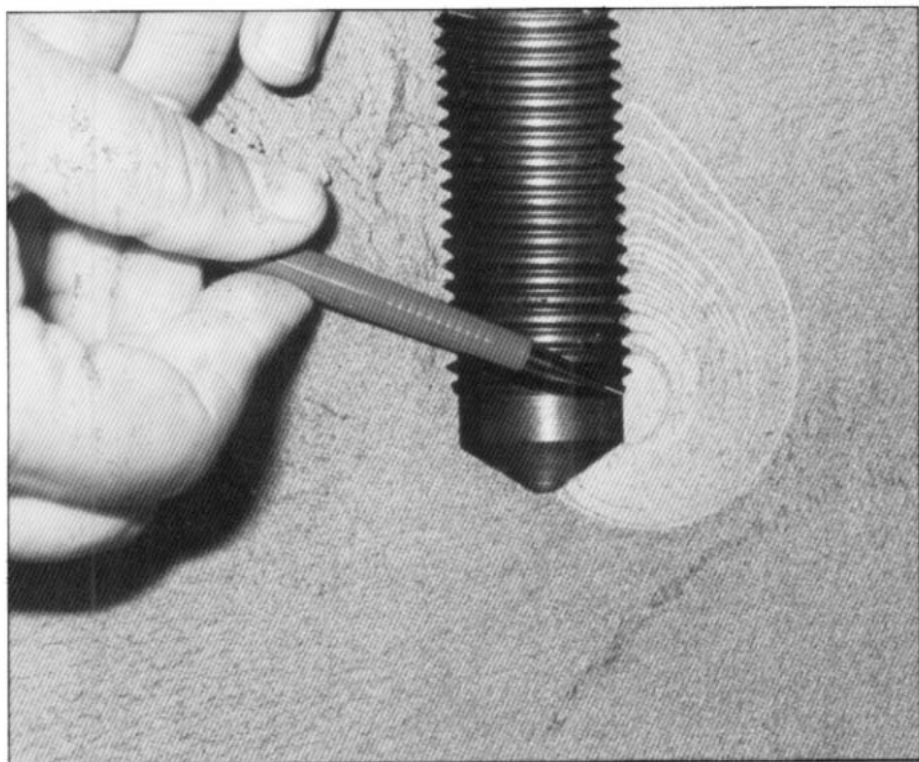


NORD

NOVEMBER 1989

CRACK ARREST

**Additional Safety
against Catastrophic Fracture**



nka

Nordic
liaison committee for
atomic energy

CRACK ARREST

Additional Safety against Catastrophic Fracture

Final Report of the NKA Project MAT 550

**Edited by
Lars Dahlberg
The Swedish Plant Inspectorate**

November 1989

PREFACE

The experimental part of this project was performed by the Norwegian Institute of Technology, the Technical Research Centre of Finland and Riso National Laboratory in Denmark. Three methods were investigated for measurement of the crack front position in the interior of a specimen. Ultrasonics and light optics at the Norwegian Institute of Technology and potential drop at the Technical Research Centre of Finland.

Numerical studies and evaluations of the experiments were performed at The Swedish Plant Inspectorate. Participants in the project are listed in the back.

Available on request from:

The Swedish Nuclear Power Inspectorate
Library
P.O. Box 27106
S-102 52 Stockholm
S w e d e n

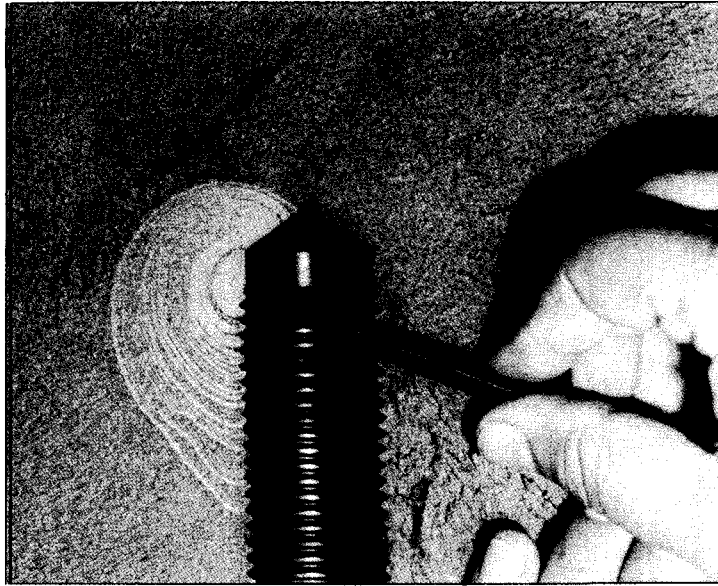
A.S. Veritec
Stig Wästberg
P.O. Box 300
N-1322 Hovik
N o r w a y

Riso National Laboratory
Christian Debel
P.O. Box 49
DK-4000 Roskilde
D e n m a r k

Technical Research Centre of Finland
Metals Laboratory
Library
P.O. Box 26
SF-02151 Espoo
F i n l a n d

ISBN 87 7303 402 9
NORD 1990:18

Graphic Systems AB, Malmö 1989



The front cover shows the surface of a fracture of a large pressurized component. First a crack developed, caused by fatigue from a small notch in the thread root (lighter parts of the fracture surface). In the later part of the fatigue growth process, unstable fracture was initiated and arrested several times before the final unstable fracture occurred (darker parts of the fracture surface).

ABSTRACT

The theory for analysis of rapid crack growth and arrest is now well developed at least for mainly linear elastic material behaviour. The dynamic fracture properties of the material must, however, be known to enable analysis of rapid crack growth and arrest and to design for crack arrest. The experimental technique for determination of these properties needs further development. Phenomena such as ligaments remaining behind the crack front and curved crack front which often occur in tough materials cause uncertainties in the evaluation of experiments. In order to increase the accuracy in the evaluations, several methods such as ultrasonics, light optics and potential drop have been tested to try to measure the crack front position in the interior of a specimen. The more developed surface method based on strain gauges was used as the reference method for measurement of the crack tip position. The dynamic fracture properties for steel A533 B C1.1 have been evaluated from experiments on large compact crack arrest specimens and compared to data reported in the literature.

KEY WORDS: Crack propagation, fracture mechanics, fracture properties, fracture toughness, materials testing, ultrasonics.

This report is part of the safety programme 1985 - 1989 sponsored by NKA, The Nordic Liason Committee for Atomic Energy. The project work has been financed in part by the Nordic Council of Ministers, and in part by The Swedish Nuclear Power Inspectorate, The Royal Norwegian Council for Science and Industrial Research, and The Minister for Trade and Industry in Finland.

SUMMARY

Structural failures are often caused by cracks or crack-like defects. Such failures can be avoided if the structures are regularly inspected in such a way that non-detected or accepted cracks are sufficiently small not to initiate and start to grow in an unstable manner. An extra safety can be achieved if it can be shown that a rapidly growing crack will stop before a catastrophic failure has developed. Since there is always some degree of uncertainty in inspection, this extra safety is of vital importance for certain structures where complete failure would be disastrous. Such structures are for instance large offshore structures, LNG-tanks, certain pipe lines and nuclear and chemical reactor pressure vessels.

The theory for analysis of rapid crack propagation and arrest is now well developed, at least for materials which mainly show linear elastic behaviour. In general finite element methods (FEM) including dynamic effects have to be used for proper analysis. Comparative dynamic analyses performed independently in this study and in a study at Oak Ridge National Laboratory (ORNL) of experiments performed within the Heavy Section Steel Technology (HSST) program gave results which showed good agreement. This gives confidence in the used analyses methods.

To enable analysis of rapid crack propagation and crack arrest and to enable design for crack arrest, the dynamic fracture properties of the material have to be known. The primary aim of this project has been to study and develop experimental techniques for determination of these properties.

Earlier experience from crack arrest experiments on tough steels such as A 533 B Cl.1 has shown that the crack front often is strongly curved. This makes surface measuring techniques for determination of the crack tip velocity less reliable.

Therefore, several methods such as ultrasonics, light optics and potential drop have been tested to try to measure the crack front position in the interior of the specimen. All three methods are shown to be useful for indication of the passage of the crack front. Further investigations of all three methods are, however, needed to clarify their full potential.

The material for the experimental part of the project, steel A 533 B Cl.1, was given by the Nuclear Regulatory Commission in the USA (US NRC) and ORNL. The steel was delivered in plates, 100 mm thick, and approximately 1000 x 500 mm large. They had been cut out from some of the fractured wide-plates used for crack arrest experiments in the HSST-program. The objective was to obtain dynamic fracture properties for the same steel from to independent investigations.

Two large compact crack arrest (CCA) specimens, 400 x 400 x 100 mm, were manufactured from each plate. A total of eight experiments were conducted, four in Norway, two in Finland and two in Denmark. The results of the experiments showed that the CCA-specimen has a suitable geometry for determination of dynamic fracture properties. A drawback is, however, that the propagating crack will experience a decreasing stress intensity factor thus somewhat limiting the level of crack arrest values that can be reached with this geometry.

The method of strain gauges was used as the basic method for measurement of crack length as function of time. The method gave distinct strain peaks which could be analysed by FEM for evaluation of the time instant of crack tip passage. The evaluation of the experiments resulted in crack propagation toughness values which, as can be expected, show an increase with increasing crack velocity. The crack arrest toughness agree well with values obtained by ORNL.

Besides the technical results, the project has also given vitality to the field of crack propagation and arrest in the Nordic countries. Both the expertise in each country and the cooperation between the four countries have gained by this project.

SAMMANFATTNING

Haverier orsakas ofta av sprickor eller sprickliknande defekter. Sådana haverier kan undvikas om konstruktioner inspekteras regelbundet på ett sådant sätt att oupptäckta eller acceptabla sprickor är tillräckligt små för att inte initiera brott. En extra säkerhetsbarriär erhålls om sprickstopppning av en snabbt löpande spricka kan tillförsäkras innan totalhaveri är ett faktum. Eftersom inspektion alltid är behäftad med viss osäkerhet är denna extra säkerhetsbarriär av stor betydelse för vissa typer av konstruktioner för vilka ett haveri skulle vara förödande. Exempel på sådana konstruktioner är stora offshore-anläggningar, LNG-tankar, naturgasledningar och reaktortankar i nukleära kraftverk och process-anläggningar.

Teorin för analys av snabb spricktillväxt och sprickstopppning är nu välutvecklad, åtminstone för material som i huvudsak är linjärt elastiska. En fullständig analys av spricktillväxtförlopp måste vanligen baseras på finit element metod och inkludera dynamiska effekter. Jämförande dynamiska analyser utförda dels i detta projekt och dels vid Oak Ridge National Laboratory (ORNL) av experiment utförda inom Heavy Section Steel Technology (HSST) programmet visar god överensstämmelse, vilket ger tilltro till analysmetoderna.

För att kunna analysera snabb spricktillväxt och sprickstopppning och för att kunna dimensionera för sprickstopppning av en eventuellt löpande spricka måste materialets dynamiska brottegenskaper vara kända. Den viktigaste målsättningen med detta projekt har varit att utveckla den experimentella metodiken för provning av dessa materialegenskaper.

Tidigare erfarenheter från sprickstopppningsexperiment på sega stål som t ex A 533 B Cl.1, visar att sprickfronten ofta är kraftigt krökt. Det gör metoder osäkra som endast mäter sprickfrontens läge på provstavens yta. Därför har tre metoder för mätning av sprickfrontens läge i det inre av en provstav studerats. Dessa är baserade på ultraljud, ljusoptik och potential drop. Alla tre metoderna är användbara för detektering av tidpunkten för sprickfrontens passage, men ytterligare studier behövs för att fullständigt klarlägga deras möjligheter.

Materialet, stål A 533 B, Cl.1, för den experimentella delen av projektet erhöles kostnadsfritt från ORNL och den amerikanska kärnkraftmyndigheten US NRC. Materialet levererades i 100 mm tjocka, c:a 1000 x 500 mm stora plattor som hade skurits ut från några av de brustna stora plattprovstavarna som används för sprickstopppningsexperiment inom HSST-programmet. Syftet var att få dynamiska brottdata för samma stål från två oberoende undersökningar.

Två stora "compact crack arrest" (CCA) provstavar på c:a 400 x 400 x 100 mm tillverkades av varje platta. Totalt åtta experiment har genomförts, fyra i Norge, två i Finland och två i Danmark. De experimentella resultaten visar att CCA-provstaven kan användas för bestämning av dynamiska brottdata. En nackdel är emellertid att spänningsintensitetsfaktorn minskar under sprickans tillväxt, vilket begränsar storleken på sprickstoppningssegheten som kan uppmätas med denna geometri.

Töjningsgivare användes som referensmetod för mätning av spricklängd som funktion av tid. Metoden gav tydliga töjningstoppar som kunde analyseras med hjälp av FEM för utvärdering av tidpunkten för passage av sprickfronten. Utvärdering av experimenten gav spricktillväxtsegheter som ökar med ökad spricktillväxthastighet. Erhållna sprickstoppningssegheter överensstämmer väl med motsvarande data erhållna vid ORNL.

Förutom värdet av de rent tekniska resultaten har projektet också bidragit till att vitalisera forskningen inom området snabb spricktillväxt och sprickstoppning i den nordiska länderna. Det har ökat kunskaperna på området i Norden och bidragit till nya kontakter och ökat samarbete mellan de fyra länderna.

CONTENTS

1.	INTRODUCTION	1
2.	THEORETICAL BACKGROUND	2
3.	EXPERIMENTAL METHODS	4
3.1	Measurement of boundary conditions	5
3.2	Measurement of crack tip position	7
3.2.1	Strain gauges	8
3.2.2	Ultrasonic transducers	9
3.2.3	Optical fibers	16
3.2.4	Potential drop	21
4.	NUMERICAL TECHNIQUE	28
5.	HSST WIDE-PLATE TESTS	31
6.	LARGE CCA-SPECIMEN TESTS	39
6.1	Quasistatic analysis	40
6.2	Dynamic analysis	45
7.	CONCLUSIONS	54
	ACKNOWLEDGEMENT	55
	REFERENCES	56
	LIST OF PARTICIPANTS IN THE PROJECT	59
	PUBLISHED REPORTS	60

1. INTRODUCTION

Structural failures are often caused by cracks or crack-like defects. Such failures can be avoided if the pressure vessels are regularly inspected in such a way that nondetected or accepted cracks are sufficiently small not to initiate and start to grow in an unstable manner. An extra safety can be achieved if an arrest of a rapidly growing crack can be assured before a catastrophic failure has developed. Since there is always some degree of uncertainty in inspection, this extra safety is of vital importance for certain structures where complete failure would be disastrous. Such structures are for instance LNG-tanks, certain pipe lines and nuclear and chemical reactor pressure vessels.

To assess the arrest capability, information of the dynamic fracture properties is needed. During recent years these properties of the steel A533B C1.1, have been the object of intense studies. Among the large scale projects in progress in this field are the pressurized thermal shock experiments at Oak Ridge National Laboratory, Bryan et al (1986), the NRC/HSST wide-plate crack arrest program at The National Bureau of Standards, Pugh, (1986 b) and the EPRI/CE crack arrest program at Combustion Engineering, Ayres et al, (1986). Apart from obtaining information of the crack propagation phase, these tests are aimed at providing crack arrest data at temperatures near the Charpy upper-shelf. This is usually achieved by using a suitable combination of specimen geometry and loading set-up causing an increasing stress intensity factor with crack length. A crack arrest is then obtained by applying a temperature gradient along the direction of crack growth and thereby causing an even steeper toughness gradient.

The primary aim of this project is to study and develop experimental techniques for determination of dynamic fracture properties. With the use of the compact crack arrest specimen (CCA-specimen) and the conventional transverse wedge loading technique, the propagating crack will experience a decreasing K-field, thus somewhat limiting the level of crack arrest toughness values that can be reached with this geometry. For higher temperatures, experience from the ASTM K_{Ia} Round Robin, Fourney and Chona (1986), has often shown strongly curved crack fronts thus making surface measuring techniques for determination of the time-dependent crack front position less reliable. Therefore, an important task within this project is to develop experimental methods to measure the crack front position in the interior of the specimen.

2. THEORETICAL BACKGROUND

Consider a Mode 1 propagating crack in a two dimensional body. Under linear elastic fracture mechanics (LEFM) conditions the following growth criterion is assumed

$$K_{I^d} = K_{pc} (\dot{a}, T) \quad (2.1)$$

where K_{I^d} is the elasto-dynamic stress intensity factor and K_{pc} is a material function depending on crack-tip velocity \dot{a} and temperature T at the position of the tip. The crack will come to a momentary stop if (2.2) is fulfilled

$$K_{I^d} < K_{Ia} (\dot{a} = 0, T) = K_{Ia} (T) \quad (2.2)$$

K_{Ia} is here termed the crack arrest toughness and is of primary interest in determining the arrest capability of a material. Since K_{I^d} depends on the entire history and not only on the instantaneous conditions, a fully dynamic analysis must in general be performed.

In a quasistatic treatment K_{I^d} is replaced by K_{I^s} , the statically calculated stress intensity factor, which only depends on the momentary conditions. This treatment is e.g. adopted in the ASTM-standard E 1221 (1988).

It is, however, important to realize that for many ductile materials, it is unlikely that the basic assumptions of LEFM are valid. An important step towards a better understanding of crack growth in non-linear materials has been the inclusion of rate effects in the plastic deformation process. Rate effects can be expected to be important because of the very high strain rates that exist in the vicinity of a running crack-tip. A number of recent investigations, both theoretical and experimental, have adopted rate dependent models for the running crack problem, e.g. Douglas (1982), Aboudi and Achenbach (1983), Lo (1983), Brickstad (1983 b), Freund and Hutchinson (1985), Freund et al (1986) and Kanninen et al (1986 b). In the investigation discussed here the authors have chosen to use the special case of Perzyna's (1966) viscoplastic material model that is described in chapter 4. It is thus appropriate to consider the energy balance for a plane body of unit thickness containing a Mode 1 propagating crack. The interest is focused on the difference between on one hand the energy input to the body and on the other hand the strain energy, the kinetic energy and the viscoplastic dissipated energy. The net change is associated with crack growth, i.e. consumed in advancing the crack. This quantity, per unit area of crack extension, represents the energy flow to the crack tip region and is denoted by γ .

The here adopted fracture criterion may be given the following form in an isothermal case

$$\begin{aligned} \gamma &= \gamma_f(\dot{a}) & \dot{a} > 0 \\ \gamma &= \gamma_f(\dot{a} = 0) & \dot{a} = 0 \end{aligned} \quad (2.3)$$

γ_f is the specific fracture energy and is regarded as a characteristic function of the material. In dynamic LEFM, dissipated energy is not considered and the resulting energy flow is then equivalent to the well known energy release rate G , which makes the energy based fracture criterion completely equivalent to a fracture criterion based on the stress intensity factor. It is not selfevident what type of criterion is most suitable to use in a non-linear case. Other criteria have been suggested, e.g. based on critical values of the crack-tip opening displacement, the crack-tip opening angle or the plastic strain.

An attractive feature with the viscoplastic material model used in this study is that for the exponent $n > 3$ in the flow rate function, see chapter 4, the near-tip field is of elastic type, Hui and Riedel (1981), McCarnety (1982), Lo (1983) and Brickstad (1983 b). This may justify the definition of a near tip stress intensity factor (K_{I}^{tip}) which may control the fracture process within the region of asymptotic elastic dominance. In general K_{I}^{tip} will be less than the remote stress intensity factor defined under LEFM conditions in eqn (2.1), since for that case plastic dissipated energy is not considered.

3. EXPERIMENTAL METHODS

It is evident from experiences reported by Bryan et al (1986), Pugh (1986 a) and Ayres et al (1986) that performing dynamically instrumented crack arrest experiments is an elaborate task, both experimentally and in the way the tests should be analysed and interpreted. In order to obtain dynamic fracture toughness properties from a crack arrest experiment, accurate measurements of the time dependent crack length or the equivalent crack velocity and from the in general time dependent boundary conditions are needed.

The specimen geometry used for the experiments in this investigation is the CCA-specimen. The loading arrangement for this specimen type is shown in Fig 3.1.

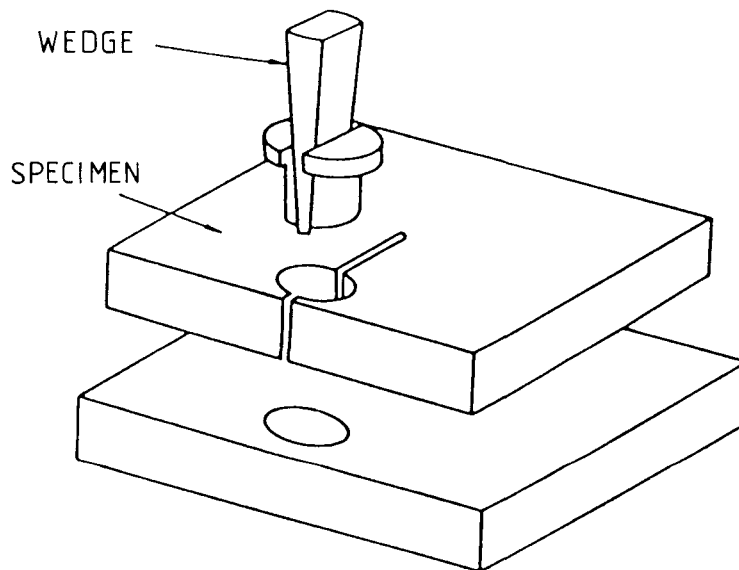


Fig 3.1 Loading arrangement for the CCA-specimen.

With this geometry the crack arrest toughness evaluated by a fully dynamic finite element analysis can be compared to the arrest toughness evaluated according to ASTM E 1221 (1988). Another reason for the choice of this geometry is that the three laboratories involved in the experimental part of this work all have earlier experience from experiments with this geometry.

3.1. Measurement of boundary conditions

A side-view of the CCA-specimen is shown in Fig 3.2.

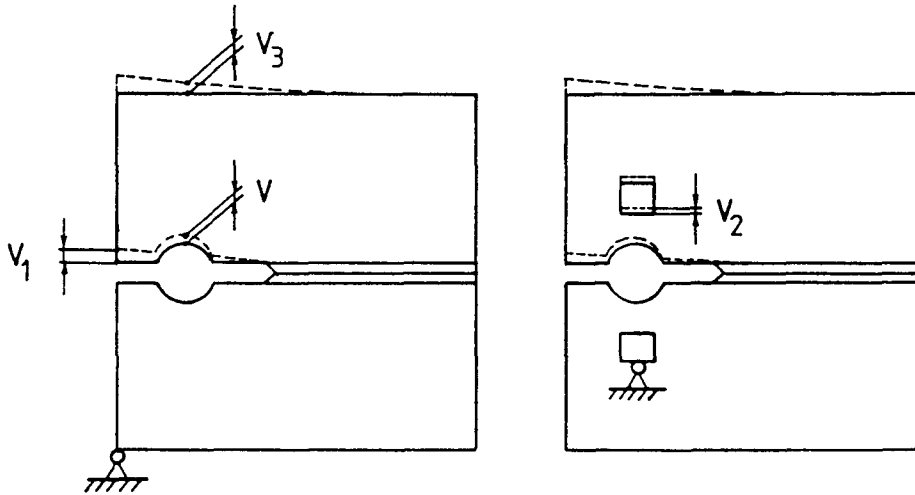


Fig 3.2 Sideview of the compact crack arrest specimen with indicated positions for possible displacement measurements.

In the CCA-specimen with the transverse wedge loading technique, the displacement is controlled in the split pin hole, see Fig 3.2. Thus it is desirable to measure the displacement v in the hole during a test. It should, however, be observed that the only geometrical constraint which is imposed on the specimen during a test, is that the specimen is not allowed to move back into the split pin. It is here assumed, that due to the short duration of the test, the wedge will not be capable to significantly increase the displacement during the crack growth event. It may of course lose contact during some part of the event, but such a behaviour will come out from the subsequent dynamic analysis.

Thus, if it is possible to obtain accurate information of the crack velocity, it is sufficient to measure the displacement v when the crack growth starts, which may be calculated from static displacement measurements at any convenient position on the specimen, for instance at v_1 , in Fig 3.2. In the subsequent evaluation the constraint condition $v \geq v(t=0)$ is then imposed in the dynamic analysis, where $t = 0$

corresponds to initiation of rapid crack growth. A main difficulty is, however, to measure the crack tip position with sufficient accuracy. In order to have more control of the process it may still be desirable to measure the displacement at some position of the specimen during the crack growth event, e.g. v_1 , v_2 , or v_3 in Fig 3.2. This measurement can be compared to the displacement at the same position obtained from the dynamic analysis. If there is a significant difference and the measured displacement is reliable, something in the input to the numerical analysis is likely to be inaccurate, probably the crack velocity.

Fig 3.3 shows an evaluation example of computed displacements at different positions of the CCA-specimen for an experiment presented by Rahka (1980).

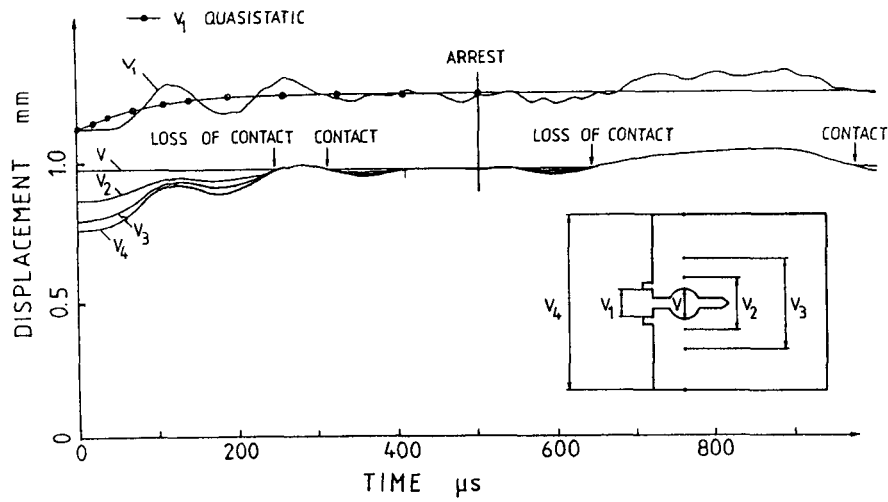


Fig 3.3 Evaluation example of displacements versus time for an experiment assuming $K_{Ia} = 65 \text{ MPa}\sqrt{\text{m}}$.

The finite element computation was run in "application mode" with the assumption of global plane strain and $K_{Ia} = 65 \text{ MPa}\sqrt{\text{m}}$. The displacement v_1 as function of time is computed both dynamically and quasistatically. It is clearly seen that v_1 increases during crack growth, although the displacement v at the hole boundary remains constant. That v_1 is greater at arrest than at initiation is also generally observed in the ASTM Round Robin tests, Fournery and Chona (1986). This is explained by the compressive stresses at the load line which relax as the crack grows. This deformation wipes out other

effects during crack growth which tend to give a contrary deformation.

It is also observed that the computed dynamic displacements v_1 are oscillating around the quasistatic curve and for these evaluations they almost coincide at the predicted time of arrest. This may not always be the case. As shown in Fig 3.3 the specimen can lose contact with the split pin during the crack growth event, thus giving a larger instantaneous displacement than the static displacement evaluated before or after crack growth.

It is interesting to note in this case, that during the time intervals when the specimen loses contact with the split pin, i.e. $v > v(t = 0)$, all the load line displacements v_2 , v_3 and v_4 coincide. This observation offers a guidance to how a proper instrumentation of the transverse wedge loaded CCA-specimen should be done in order to measure the displacement controlled boundary conditions. First the displacement v at initiation ($t = 0$) is determined. Up to this point static conditions prevail.

During crack growth and arrest, the displacement V_{LL} at some position along the load line is measured. If V_{LL} is less than $v(t = 0)$ the specimen should be in contact with the split pin and thus $v = v(t = 0)$. If $V_{LL} > v(t = 0)$ the load line displacement V_{LL} can be used directly, i.e. $v = V_{LL}$. An evaluation of K_{Ia} according to the ASTM E 1221 procedure (1988) where the displacement is evaluated some time after crack arrest can thus be inaccurate if the specimen loses contact with the split pin at the occurrence of crack arrest. Using V_{LL} in the evaluation as described above gives probably a better estimate in such a case.

3.2 Measurement of crack tip position

One of the fundamental parameters in rapid crack propagation theory is the crack velocity which can be calculated from measurement of the crack length as function of time during a crack propagation event. Determination of the crack velocity is essential for generating data of the crack propagation toughness of the material. Discrete ladder gauges, conducting foils attached to the specimen surface, high speed photography and strain gauges are some of the methods used for this purpose.

However, they all measure the crack propagation at the specimen surface or close to it. This may cause large errors when crack tunneling effects are present, i.e. when the crack extension in the interior of the specimen is significantly different from the extension at the surfaces. Such nonuniform crack growth has often been observed for the A 533 B Cl. 1 steel at and above the Charpy transition region, see for

instance the results from the ASTM Round Robin program on crack arrest testing, Fournery and Chona (1986). In this section three methods for measurement of crack extension in the interior of the body, ultrasonic transducers, optical fibers and potential drop are described together with some experimental results. The used surface method based on strain gauges is also briefly presented.

3.2.1 Strain gauges

This method is proven, with simple interpretation of recorded data, Naus et al (1987). The theory behind the use of strain gauges is described by Dally and Sandford (1987).

As the advancing crack passes under a strain gauge, a peak occurs in the strain time output response of the gauge. Knowing the strain gauge locations and the time at which the strain peaks occur, the average crack velocity between reference points can be estimated.

A recommended position of the strain gauges is at a distance

$$h = B/2 + (B - B_N)/2 \quad (3.1)$$

away from the side groove. With $B = 100$ mm and $B_N = 84$ mm h equals 58 mm. In this investigation four to six strain gauges were used on each specimen. An example of the location is shown in Fig 3.4.

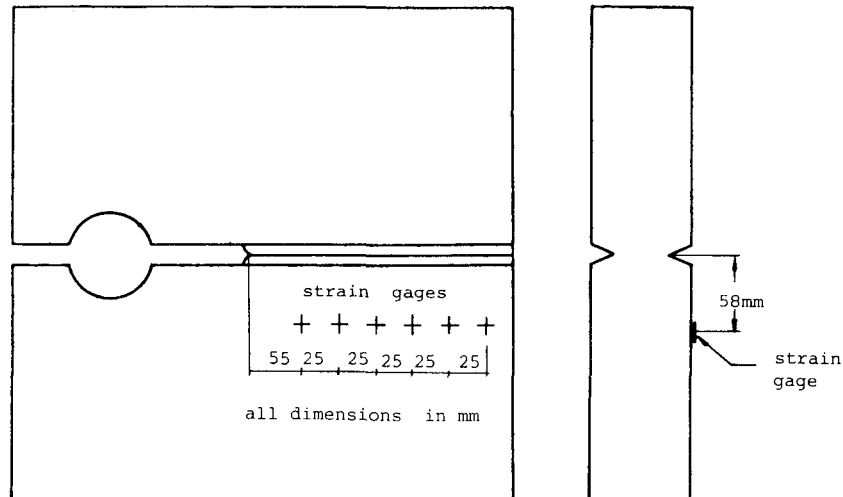


Fig 3.4 Location of strain gauges in the SINTEF specimens.

3.2.2 Ultrasonic transducers

This technique is described in more detail by Lundberg and Bryne (1988). The basic principle is quite simple. Ultrasonic waves are transmitted through a specimen, see Fig 3.5. During crack propagation the amplitude reaching the receiver will be reduced due to reflection of the ultrasonic waves at the crack surface. The time instant of this event can be recorded by a transient recorder. The crack velocity can be estimated if a series of transducers are mounted along the expected crack path.

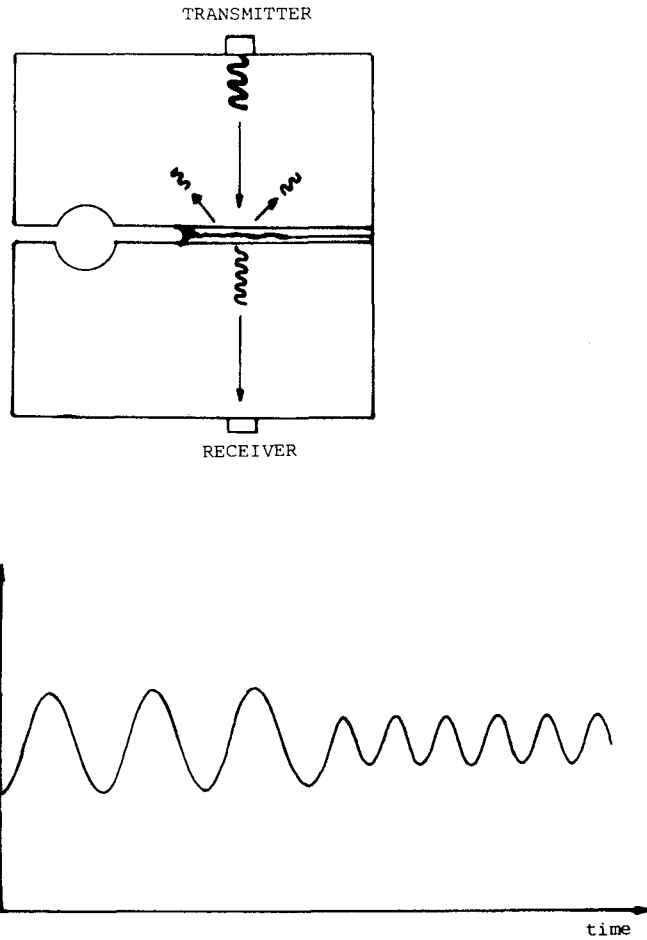


Fig 3.5 Ultrasonic wave during crack growth.

In early days of non-destructive testing, continuous ultrasonic waves were used, with flaw detection being based on a decrease in radiation intensity. This approach had some major difficulties, such as generation of standing waves, which created phantom echoes and lack of acoustic transparency of certain thicknesses of materials. With the pulse echo concept these difficulties could be overcome and today the pulse echo method is predominant.

In this application of ultrasonics it is, however, not the detection of a flaw that is important but detection of the crack history, i.e. to determine the time instant when the crack passes the ultrasonic transducers. For this purpose the pulse-echo concept does not work well due to the intermittent nature of the ultrasonic signals, Fig 3.6. The continuous wave concept is preferable.

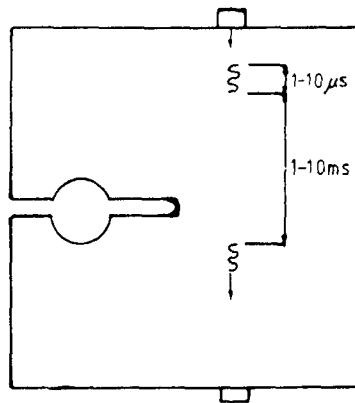


Fig 3.6 The pulse-echo concept is not suitable for detection of crack tip passage. With a velocity of 500 m/s and a pulse repeating frequency of 1 kHz the crack will travel 0.5 m between two pulses.

In this investigation, the transducers were mounted as shown in Fig 3.7. The brackets were made of the same material as the specimens to avoid difference in acoustic impedance. Furthermore, to avoid interference between the ultrasonic waves from adjacent transmitters every other is placed at the opposite side of the specimen.

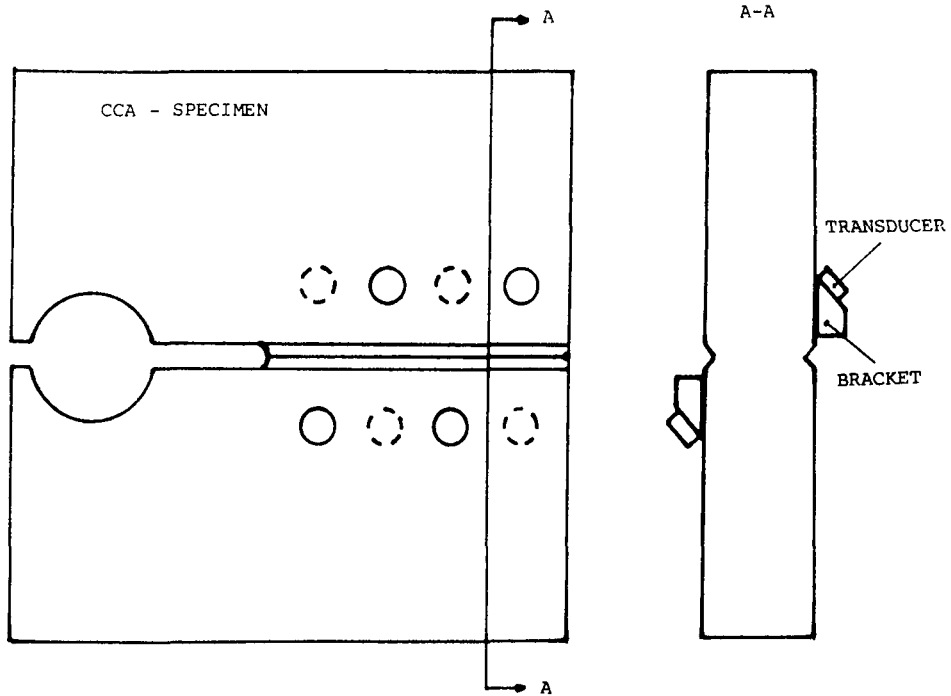


Fig 3.7 Position of the ultrasonic transducers.

The experimental set up is shown in Fig 3.8. As can be seen all the ultrasonic transmitters were fed by one signal generator, which delivered 10 V peak to peak sinusoidal. At the receiver side the signal had dropped to 0.5 - 2.0 V. The oscilloscope was used to check the signals before the test run. The natural frequency of the transducers is 2.0 MHz. To get a signal as strong as possible through the specimens, the signal generator had to be tuned to about 2.2 MHz. The test run was registered in a four channel transient recorder at a sampling rate of 10 MHz and with a memory of 10 K per channel.

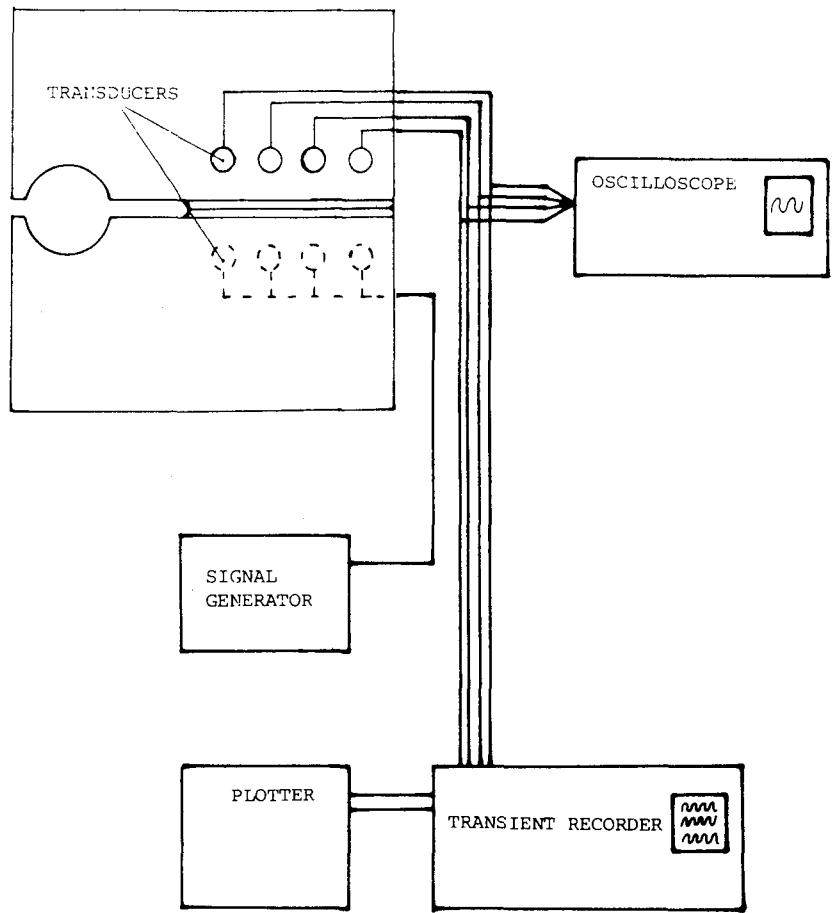


Fig 3.8 Experimental set-up, schematically.

The transducers used ranged from simple piezoelectrical circular plates to professional types with focusing beams. The ultrasonic waves, with a frequency of about 2 MHz require a sampling rate ten times as high to get a good record. This gives a total recording time of 5 ms including pretriggering. It is too short to get all the interesting oscillations on the record.

Another and greater problem is the ultrasonic noise in the specimens. The crack propagation creates acoustic emission

including frequencies about 2 MHz which will interfere with the ultrasonic waves. From this noise, standing waves and phantom echoes are created that make interpretation of the recorded signals very difficult.

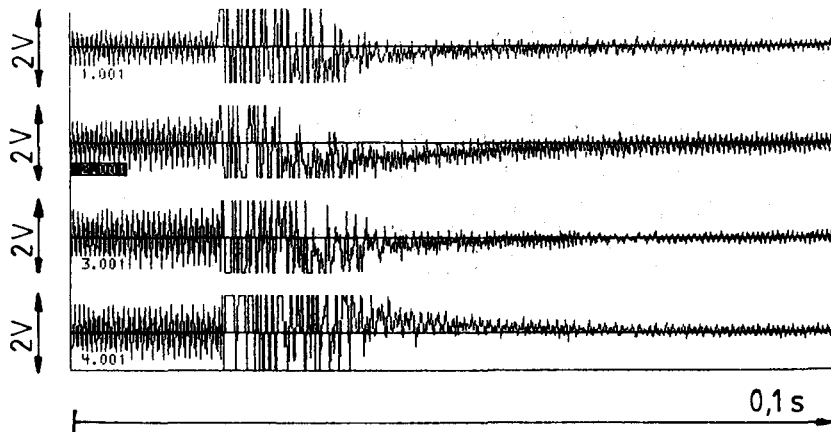


Fig 3.9 Four channel ultrasonic recording, sampling rate 100 kHz.

Fig 3.9 shows the result from a four channel recording. The sampling rate is only 100 kHz, which gives a poor record of the waves. For small times, the stress waves from the crack initiation and propagation have not reached the receivers. Only the ultrasonic waves from the transmitters are measured. When the stress waves reach the receivers, the measured amplitude is increased rapidly. The electronic circuit gets into saturation and makes any interpretation impossible.

After crack arrest the stress waves are damped out and the amplitude is reduced to a value smaller than the initial one. This confirms the basic idea of the method. The interference of the stress waves makes, however, an evaluation of the time instant of reduction of the amplitude of emitted ultrasonic waves very difficult.

To get a better recording, the sampling rate was increased to 10 MHz, Fig 3.10.

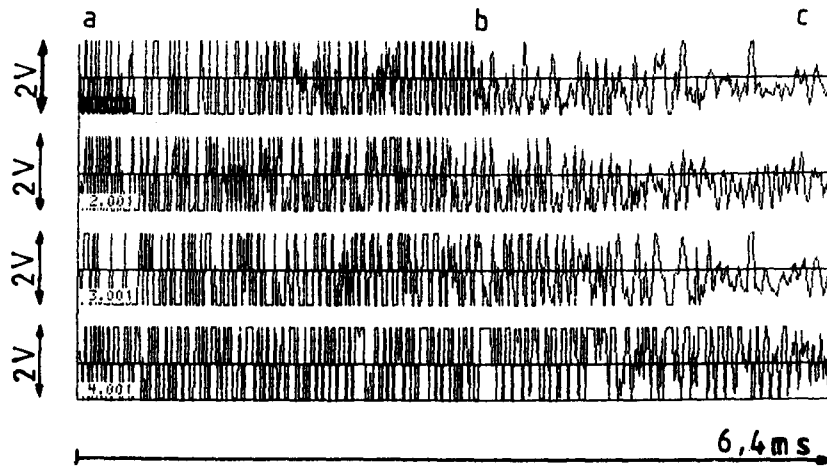


Fig 3.10 Four channel ultrasonic recording, sampling rate 10 MHz.

Three parts were cut out and enlarged in Fig 3.11.

- a) From the beginning of the record where the stress waves just begin to interfere with the ultrasonic waves.
- b) In the middle of the recording.
- c) At the end when the stress waves are dying out.

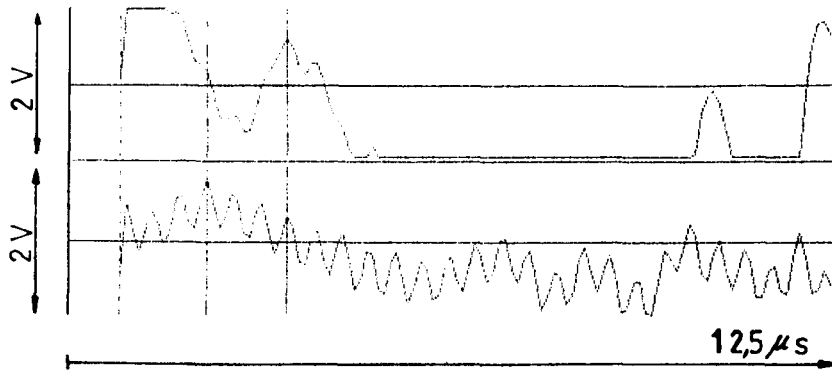


Fig 3.11 a Enlarged cut out from Fig 3.10, channel one and two.

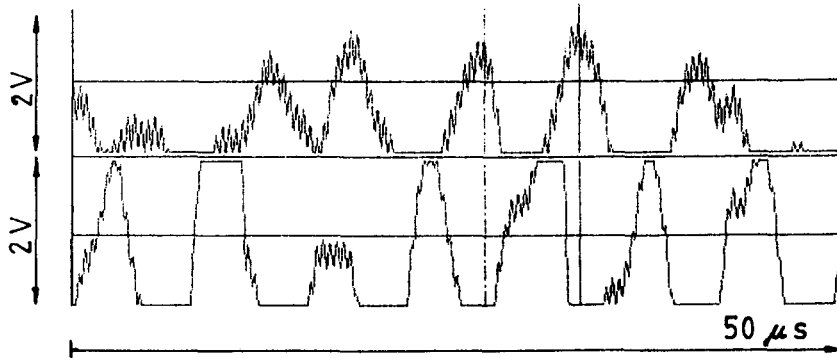


Fig 3.11 b Enlarged cut out from Fig 3.10, channel one and two.

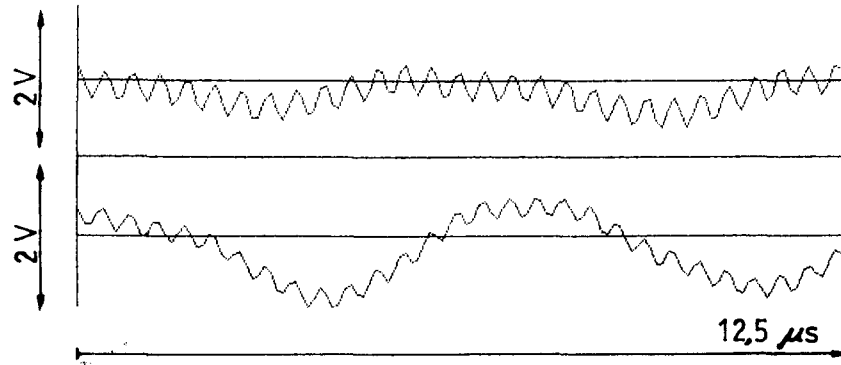


Fig 3.11 c Enlarged cut out from Fig 3.10, channel one and two.

The three Figs 3.11 a, b and c are enlarged parts from the recordings in channel one and two. The enlarged parts are marked with the respective letters in Fig 3.10. Fig 3.11 a shows that the stress waves have reached the first receiver, but not the second. The signal in channel one is greatly influenced by the stress waves, while the signal in channel two is almost undisturbed. Fig 3.11 b shows that the amplitude of the ultrasonic waves superimposed upon the stress waves is reduced. Hence, at this time the crack front has passed the transducers. The influence of the stress waves is strong. A scanning through the record, looking for the onset of reduction of the ultrasonic waves shows that the influence of the stress waves is even stronger at other time points. This makes an interpretation very difficult. Figs 3.11 b and c clearly show differences of the frequency of the stress waves and the ultrasonic waves. A further development would be to put a selective filter for the frequency of the ultrasonic waves. That might give signals easier to interpret.

The investigation can be summarized as follows:

- i) The amplitude of a continuous ultrasonic wave is reduced as the crack front passes the transducers.
- ii) Stress waves from the crack initiation and propagation interfere with the ultrasonic waves and make interpretation of the recordings difficult.

3.2.3 Optical fibers

The basic idea of this technique is that optical fibres are glued in holes which cross the expected crack growth plane in

the specimen. Light is transmitted through the fibres and an indication is obtained if the fibres fracture as the crack front passes. The technique is described in more detail by Melve et al (1987).

Holes with a diameter of 2 mm were drilled through the crack plane, see Fig 3.12. If the holes are tilted about 45 degrees to the crack plane, the machining will be easier due to shorter holes. Optical fibres with a diameter of 0.125 mm were glued in the holes with a brittle adhesive (Hotting Baldwin x-60). The holes were completely filled with the adhesive. Light from light emitting diodes (Honywell Optoelectronics SE 3362) was transmitted through the fibres and registered with high speed photodiodes (Optoelectronics SD 3478) with response time 5 ns. The voltage from the photodiodes is proportional to the received intensity of the light. Changes in transmission can then easily be registered. The experimental set up is shown schematically in Fig 3.12.

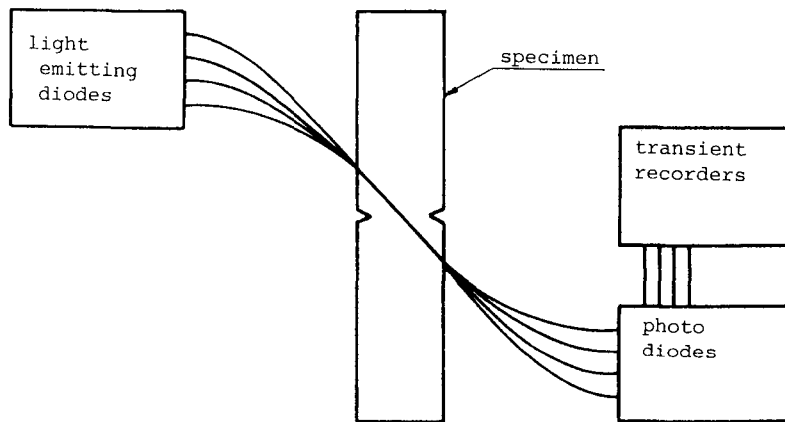


Fig 3.12 Experimental set up for optical fibres, schematically.

In general the fibres did not fracture as the crack front passed, they were only stretched. This is partly believed to be due to lack of sufficient filling of adhesion between the specimen and the fibre. Instead of a complete drop of the signal due to fracture, only a reduction of the signal was observed when a fibre was stretched.

With a thinner hole of approximately the same diameter as the fibre it is more likely that it breaks when the crack passes.

The bond to the specimen will be more stiff and the elastic properties of the adhesive less important. The problem is to drill such a thin hole through a thick specimen.

The voltage output from the four photodiodes were fed into two-channel transient recorders operating in master slave mode with sampling rate 1 MHz.

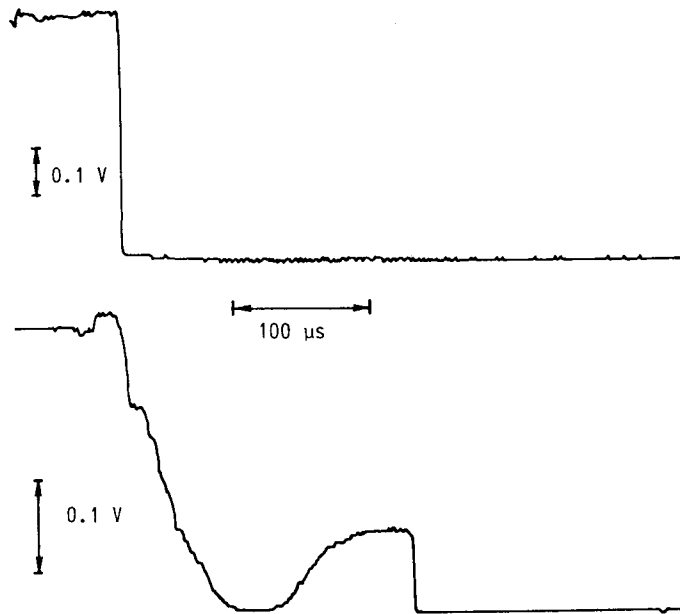


Fig 3.13 Signals from the first and the last fibre of a $W = 100$ mm duplex specimen, distance 31 mm between the fibres.

The signal recorded from fibre 1 and 4 in a duplex specimen tested at -40°C is presented in Fig 3.13. A mean velocity of 380 m/s is obtained if the crack front position is correlated to the first main drop in the signal.

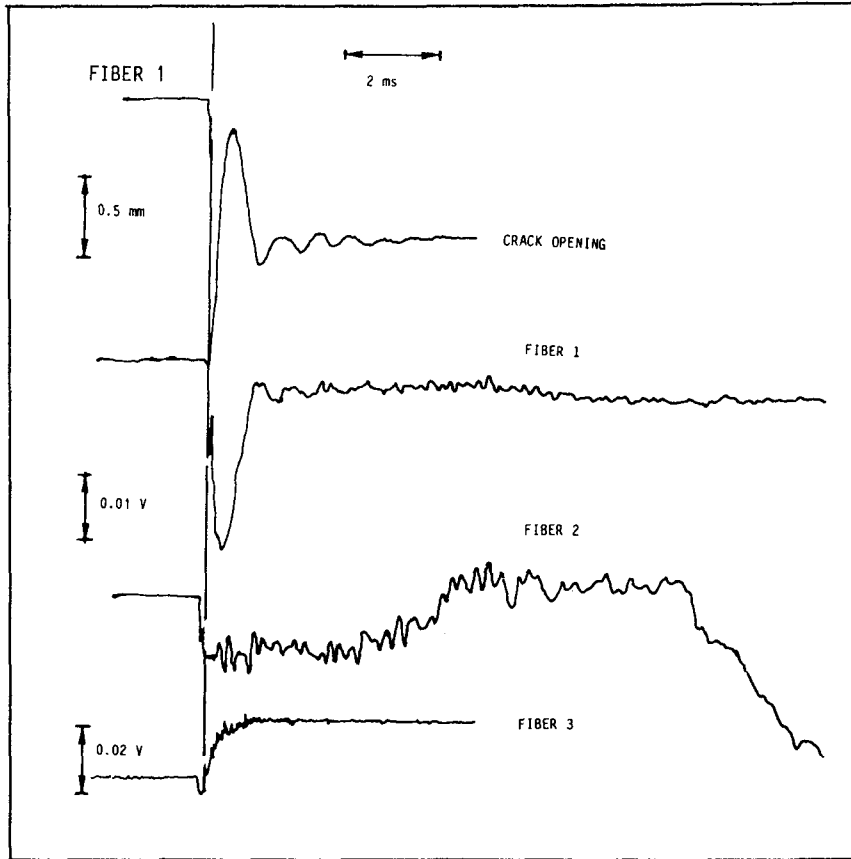


Fig 3.14 a Signals from the three first fibres and crack opening displacement of a MRL specimen with $W = 170$ mm. Duration 8 ms.

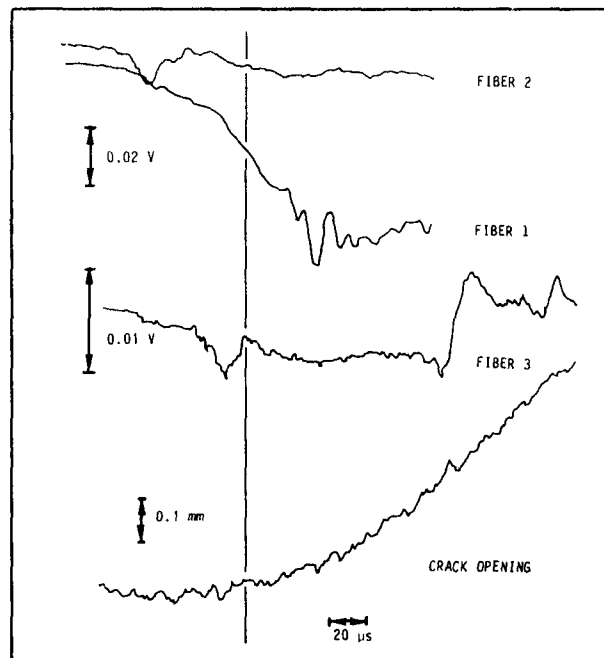


Fig. 3.14 b Same output as Fig. 3.14 a, but now with a duration of 256 μ s. The main change in fibre signals has passed before any significant opening of the crack can be observed.

In Figs 3.14 a and b are shown the signals from the three first fibres, positioned 22.5 mm apart, in a MRL-specimen with $W = 170$ mm and tested at -40°C . The crack opening displacement is measured 10 mm from the crack tip with an Eddy current displacement transducer. None of the fibres broke completely even though the crack front passed them, but a change in signal level was recorded from all fibres. It can be seen in Fig 3.14 a that the crack opening displacement was oscillating with a frequency of approximately 1.4 kHz and that the signal in the first fibre changes with the same frequency but out of phase, i. e. opening of the crack corresponds to a decreased signal due to stretching of the fibre.

An increase of the fibre strain gives a slight change in the refractive index of the glass and a reduction in the transferred light. When the strain is relaxed the transferred light increases again.

In Fig 3.14 b it is seen that the drop in fibre signals has passed before the increase in the crack opening displacement is significant. From the records it can be concluded that something have disturbed the fibres. This can only be the crack front passage.

No disturbances in the course of fracture or on the fracture surfaces could be observed due to the holes.

The investigation can be summarized as follows:

- i) Due to the relatively large holes compared to the fibres and the problems with the adhesion between the fibres and the specimens, complete fibre breakage was not always accomplished. This problem can probably be solved if smaller holes of approximately the same diameter as the fibres are used.
- ii) Signal changes due to crack propagation were observed. The crack front position as function of time can probably be evaluated from these signals.

3.2.4 Potential drop

A rapidly running crack causes a transient potential peak at the crack mouth even when direct current feeding of the specimen is used, Congleton and Denton (1977). The direct current potential drop has earlier been measured on steel specimens sized 200x200x50 mm, Rahka (1989), and now in this series on specimens sized 400x400x100 mm approximately. One potential signal was measured in the earlier experiment, Rahka (1989). It was found to be phased with the crack mouth opening vs time in a manner suggesting that the potential drop "feels" the formation of new decohesion by cleavage even occurring at some distance from the electrode, Fig 3.15, Rahka (1989).

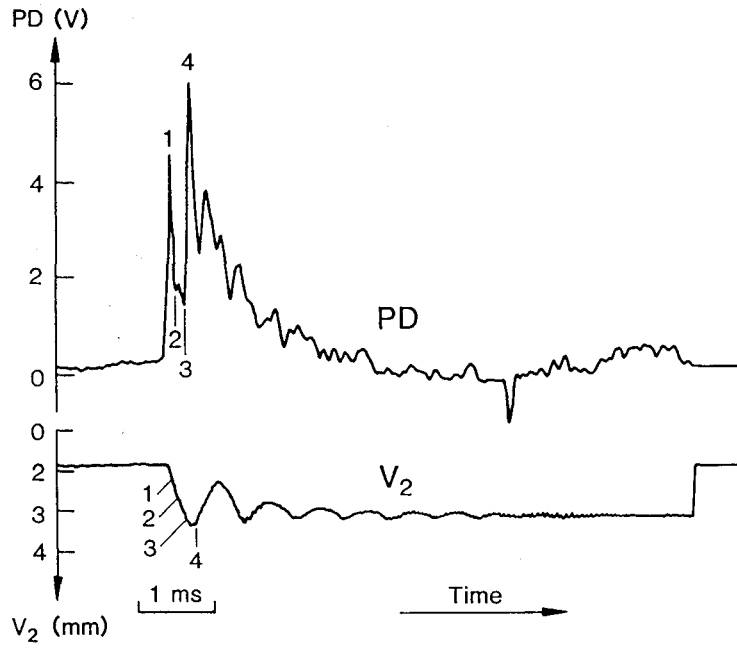


Fig 3.15 Potential drop (PD) and crack mouth opening (V) signals during cleavage crack growth in a wedge loaded compact specimen of low-carbon steel with direct current feeding, Rahka (1989)

In the tests on the larger CCA-specimens performed in this investigation, multichannel measurement of potential drop was performed. New, multichannel amplifiers were built to increase the time response (courtesy Henrik Sundell, VTT). The rise time curve for the new potential drop amplifiers is shown in Fig 3.16.

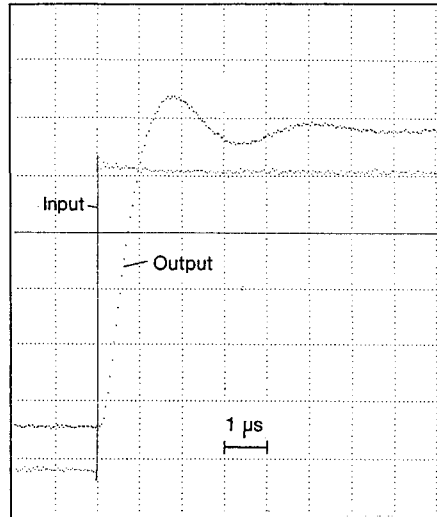


Fig 3.16 Rise time curves for the potential drop amplifiers.

In addition, dynamic crack opening behaviour was recorded as has been done earlier, Rahka (1980). A new eddycurrent sensor was acquired for this purpose (μE) with a multifold higher speed compared to the earlier sensor (DYMAC, 3 dB at 11 kHz). Both sensors were used in parallel. Strain measurements were performed on one side face of the specimen, as has been described in section 3.2.1. During testing all signals were recorded on magnetic data tape using commercial equipment (TEAC, video tape). The signals were then later plotted using a digital transient recorder (Tektronix). The positions of the various sensors in specimen VTT 2 are shown in Fig 3.17.

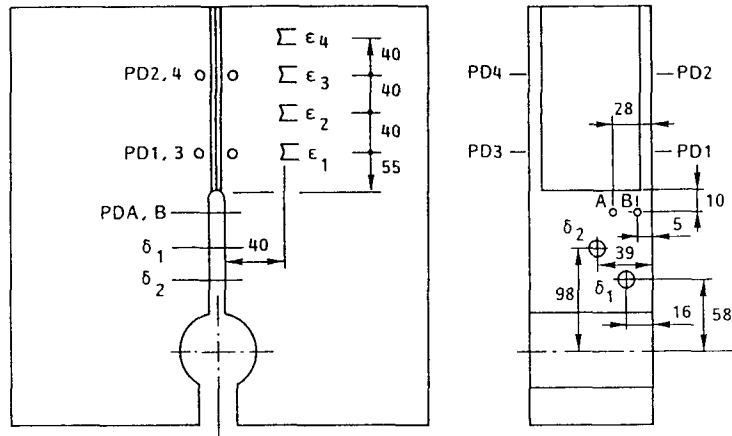


Fig 3.17 Positioning of the various sensors in specimen VTT 2

While one of the tests (VTT 1) failed to produce a satisfactory recording due to operator inexperience with the new equipment the second was successful. The potential drop electrodes on each side face were placed on the edges of the side grooves. All potential signals are shown in Fig 3.18 from the second test (VTT 2).

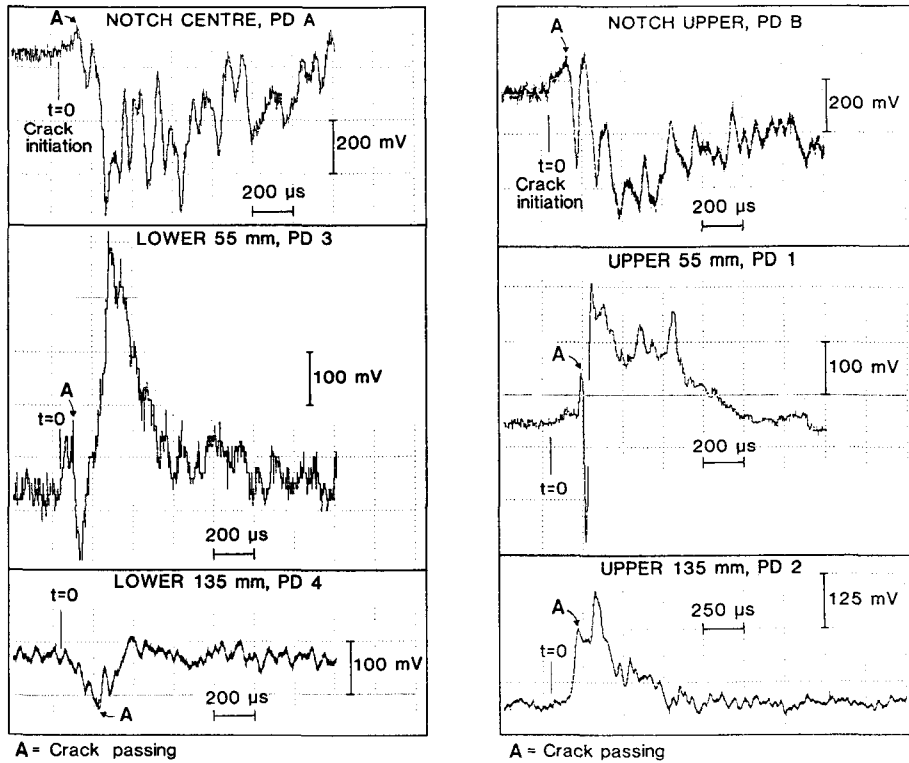


Fig 3.18 Potential drop signals measured during the run arrest sequence of cleavage fracture in specimen VTT 2.

In addition to potentials and strains two crack opening signals (δ_1 - μ E and δ_2 -DYMAG) were recorded. On all signal vs time curves, time zero has been marked based on the signal that first reacted. This was PD3 on the lower side of the specimen, 55 mm ahead of the point of crack initiation in the direction of principal crack propagation

It is of interest to note that crack initiation occurred on the upper side of the notch on test VTT 1 but on the lower side of specimen VTT 2, see Fig 3.19.

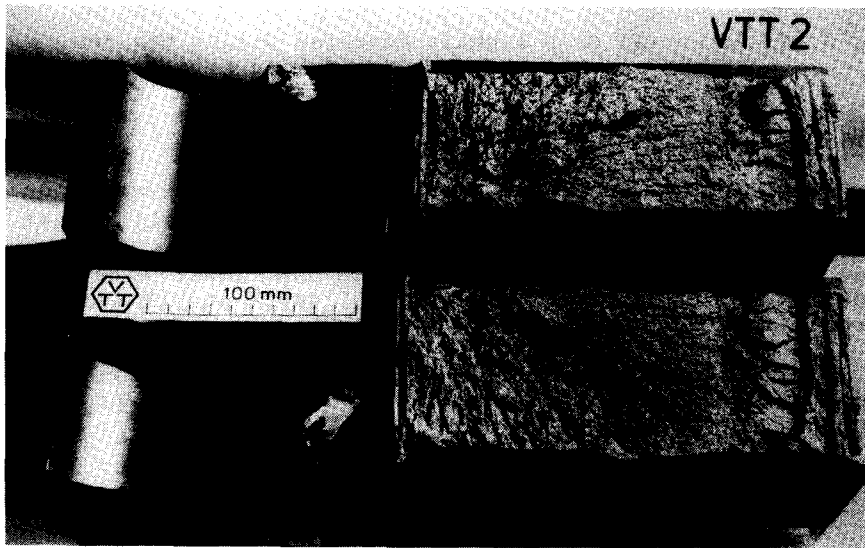
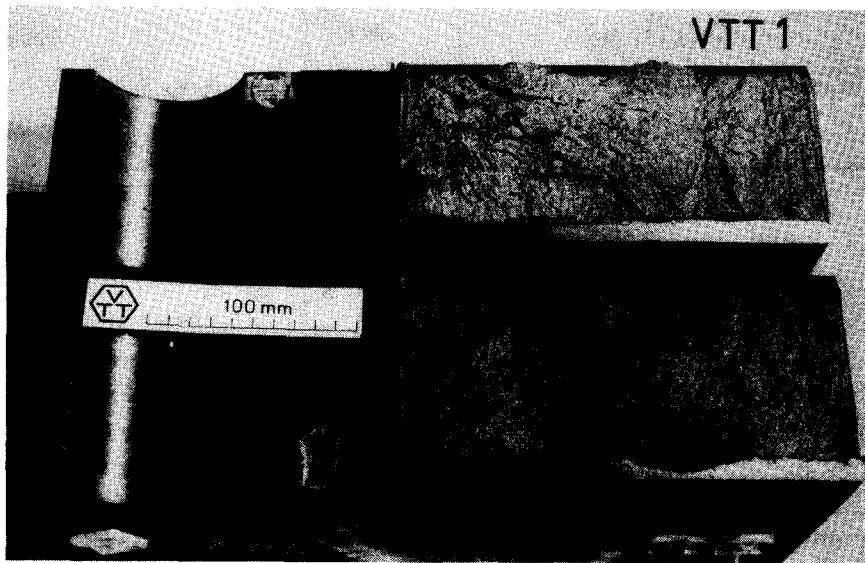


Fig 3.19 Fracture surfaces of tested large specimens VTT 1 and VTT 2.

The location of initiation was at the starting end of the notch tip embrittled weld (Hardex N, preheat 150°C) on specimen VTT 1 but at the finishing end of the embrittled weld in specimen VTT 2. However, one "long" side corner of the side face of the specimen where the crack initiated in both specimens had been flame cut before machining of the specimen. The cut was left from the mother block from which the specimens had been machined, suggesting an influence of residual stresses along the side face of the specimen close to which the initiation of cleavage occurred.

Based on the potential drop and the strain gauge outputs a cracking map has been estimated, Fig 3.20. The earliest reaction of any potential electrode has been taken as the time point of cleavage initiation (in this case PD3) and a reversing of the PD signal as the time point when the crack front passes the location of the electrode.

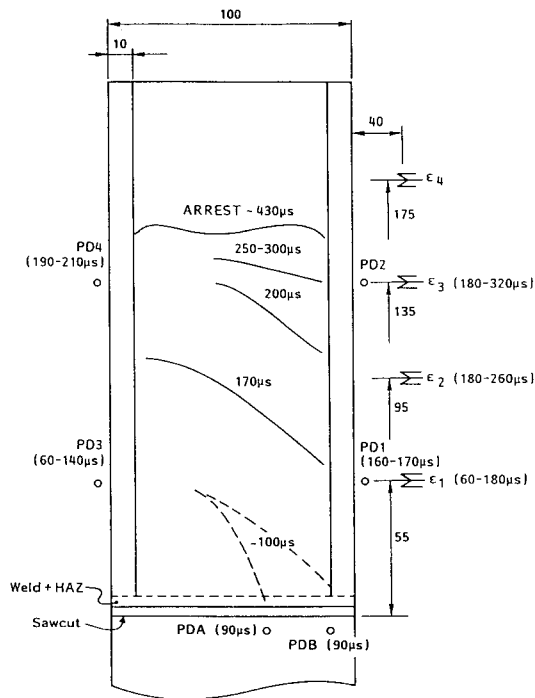


Fig 3.20 Estimated cleavage front isochrones for test VTT 2. Estimate based on Potential Drop and side face strain recordings.

4. NUMERICAL TECHNIQUE

The numerical analysis involves the solution of a time-dependent boundary value problem consisting of a crack moving through a continuous body subjected to arbitrary mechanical and/or thermal loading. For this purpose an efficient dynamic, two-dimensional, finite element program has been developed, using an explicit method based on the central difference approximation to integrate the equations of motion. The crack growth model adopted is the well established gradual nodal relaxation technique, introduced by Rydholm et al (1978), see Fig 4.1.

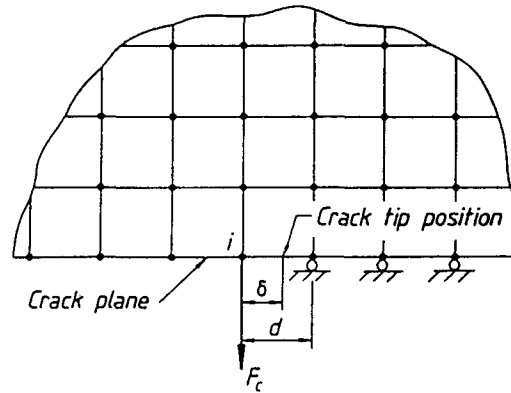


Fig 4.1 Crack growth model in the finite element mesh.

A closing force F_C is introduced behind the crack-tip. The magnitude of F_C depends on the crack-tip position $\delta(t)$ within the finite element distance d as

$$F_C = F_0 (1 - \delta(t)/d)^{0.5} \quad (4.1)$$

Here F_0 is the force in this node immediately before the relaxation begins. F_0 is thus gradually relaxed to zero as the crack propagates through the element length d . $\delta(t)$ is a known function of time if the crack velocity \dot{a} is known.

For elastodynamic applications the dynamic energy release rate G is then obtained by calculating the work performed by F_C over the finite distance d according to eqn. (4.2).

$$G = \frac{2}{d} \int_{t_i}^{t_i+d/\dot{a}} F_C(t) \dot{u}_i(t) dt \quad (4.2)$$

Here t_i is the time when the crack-tip passes node i and \dot{u}_i is the vertical velocity of this node. By utilizing the well-known relation (4.3), the dynamic stress intensity factor K_{I^d} is obtained.

$$G = \frac{K_I^2}{E} g(\dot{a}) \quad (4.3)$$

g is a universal function of \dot{a} as given e.g. by Nilsson (1975). The described procedure of evaluating K_{I^d} has shown good agreement with analytical solutions, c.f. Rydholm et al (1978). If side grooves are used the simple correction $\sqrt{B/B_N}$ is used on K_I , where B is the unnotched thickness and B_N is the thickness of the side-grooved crack plane.

Since no energy is consumed for a stationary crack, the nodal relaxation method can not be used for calculation of K_{I^d} after a crack arrest. Instead, a technique first introduced by Walsh (1972) was used to evaluate K_{I^d} . It utilizes the relation between K_{I^d} and the time dependent crack opening displacement (COD), obtained from the finite element solution, see e.g. Brickstad (1983 a) for a more detailed description.

To obtain some idea of the role of rate-dependent plasticity, some evaluations are performed using Perzyna's viscoplastic model, Perzyna (1966). A yield condition of the von Mises type which governs the initiation of viscoplastic flow is then introduced as

$$\bar{f} = f(\sigma_{ij}, \epsilon_{ij}^{vp}) - f_0 = 0 \quad (4.4)$$

where f_0 is the uniaxial yield stress, possibly dependent of some hardening parameter. Continuous viscoplastic flow is assumed to occur only when $\bar{f} > 0$ which means that stress states outside the static yield surface are admissible. The viscosity effects are introduced by the following associated flow rule.

$$\dot{\epsilon}_{ij}^{vp} = \begin{cases} \beta \phi(f) \frac{\partial f}{\partial \sigma_{ij}} & f > f_0 \\ 0 & f \leq f_0 \end{cases} \quad (4.5)$$

Here β is a fluidity parameter and Φ is a flow rate function. A choice favoured in many investigations is

$$\Phi(f) = \left(\frac{f - f_0}{f_0} \right)^n \quad (4.6)$$

in which the magnitude of the viscoplastic strain rate is assumed to be a function of the excess stress above the static loading surface, raised to some power n . The material parameters β, n and f_0 are to be obtained from experiments at different loading rates. Such experiments for the A533 B steel have been performed by e.g. Kanninen et al (1986 a). The energy flow γ to the crack-tip region which is used as a fracture criterion in eqn (2.3), is then calculated by the same technique as in the elastodynamic case and converted to some measure of the near-tip stress intensity factor by the relation (4.3) with G replaced by γ . More information of the dynamic finite element program that has been developed for the running crack problem can be found in papers by Brickstad and Nilsson (1980) and Brickstad (1983 b).

5. HSST WIDE-PLATE TESTS

In the crack arrest studies that are being conducted by the Heavy Section Steel Technology Program (HSST), crack arrest data are generated over a range of temperatures, cf Pugh (1986) and de Wit et al (1985). The material used for the first series of tests (WP-1) is A533 B Cl.1. Some of the cracked halves from these experiments are used for the Nordic crack arrest project.

The cooperation with the Oak Ridge National Laboratory (ORNL) has led to the opportunity for SA to participate in some of the numerical analyses of the wide-plate crack arrest tests. Apart from the possibility to calibrate our evaluation methods with other analysis groups, these analyses can also give valuable information of the dynamic fracture properties of the test material to be compared with the nordic crack arrest test results. In this section such analyses of wide-plate test 1.2 and 1.5 are briefly described.

Fig 5.1 shows the geometry for wide-plate test 1.2 together with the two-dimensional finite element mesh used. A plate of size 1 x 1 m of the test material A533 B is welded to pull-plates which together forms a long specimen of 9.6 m between the loading points. The initial crack length is 200 mm. A similar geometry was used for wide-plate test 1.5.

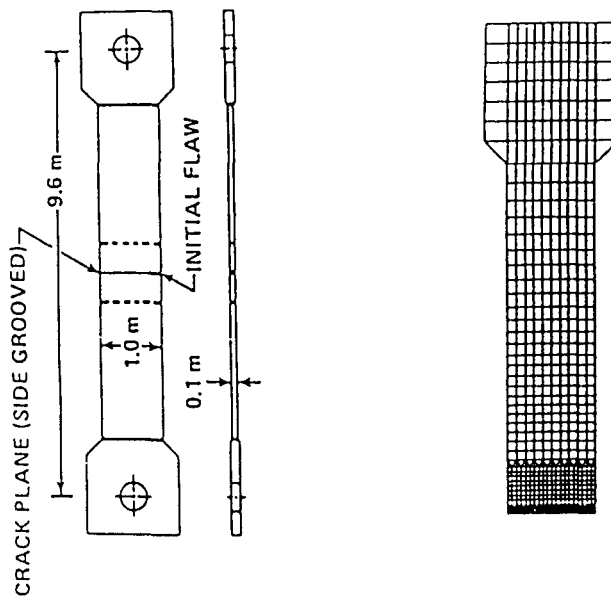


Fig 5.1 Geometry and finite element mesh for WP-test 1.2

To achieve a positive gradient in toughness, the cracked side of the plate was cooled while the opposite side was heated. A nearly linear temperature gradient over the width was obtained varying from approximately -100°C to $+200^{\circ}\text{C}$ from one side to the other for both the plate in WP-1.2 and 1.5. By imposing a slow constant displacement rate of the cross head, the specimens were then loaded until fracture occurred. As the crack propagates into a successively tougher material, the conditions for crack arrest are favourable. The specimens were instrumented with thermocouples for temperature measurements and load cells for load registration. The crack-tip position was recorded using the strain gauge technique. Fig 5.2. shows the crack length, normalized with plate width w , versus time for WP-1.2 and 1.5.

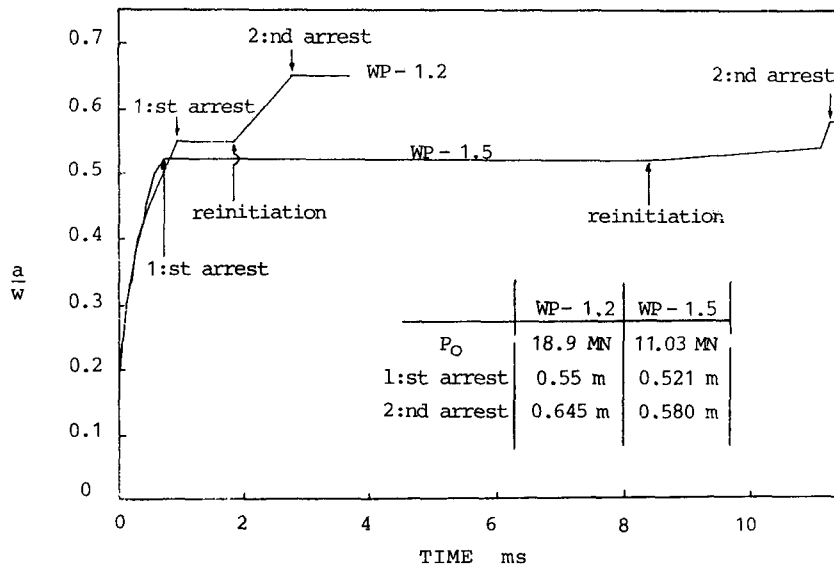


Fig 5.2. Normalized crack length versus time for wide-plate test 1.2 and 1.5.

From the recorded signals, two events of crack arrest could be deduced with a period of rest and reinitiation in between. The maximum crack velocity was estimated to 800 m/s.

The two tests have been numerically evaluated in a generation mode and using a finite element mesh of the type displayed in Fig 5.1. A mesh refinement study has also been performed using quadratic elements along the crack plane of a size $d/w = 1/40$ and $1/80$. Before the run-arrest events were evaluated the thermal deformation of the plate was determined. This deformation implied a bending of the plate which caused an eccentricity of the load-line compared to the vertical middle section of the plate at the crack plane. During the propagation event fixed displacement conditions at the loading point was assumed according to the value that corresponded to initiation of crack growth. The elastodynamic result in terms of the dynamic stress intensity factor versus time is shown in Fig 5.3 and 5.4.

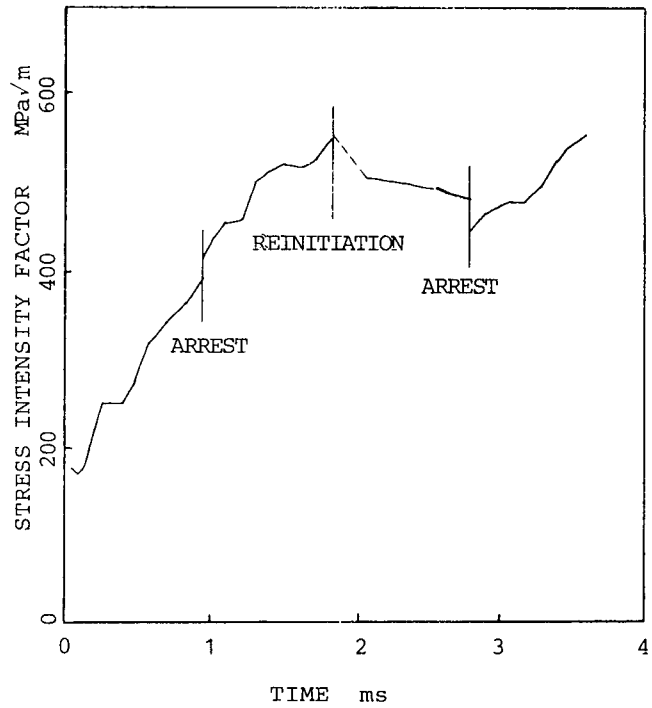


Fig 5.3 Elastodynamic stress intensity factor versus time for wide-plate test 1.2.

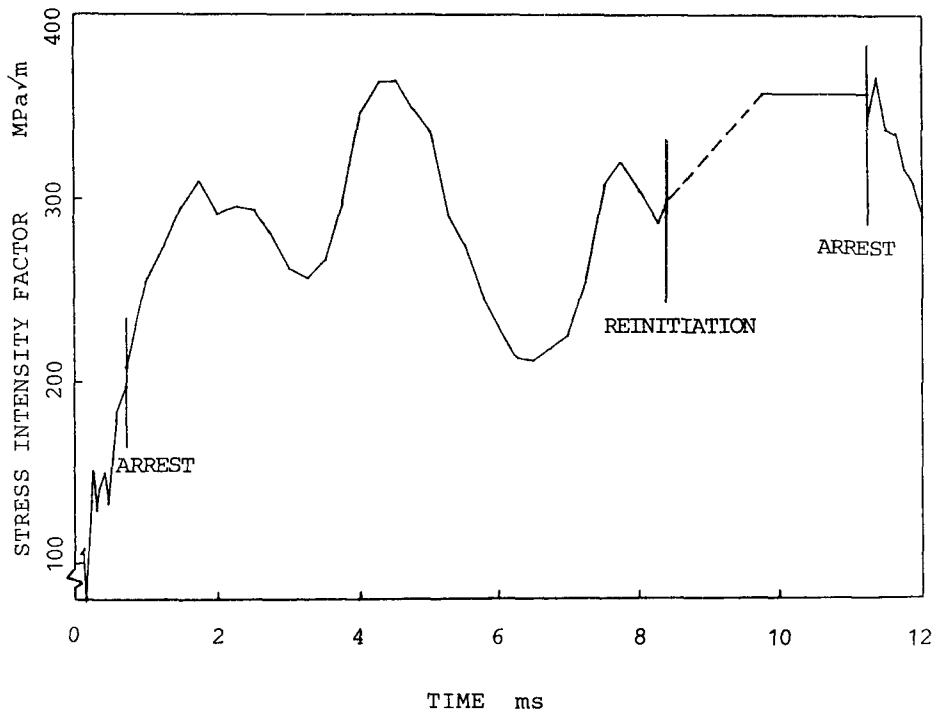


Fig 5.4. Elastodynamic stress intensity factor versus time for wide-plate test 1.5.

The elastodynamic results compare well with the analyses performed by ORNL, cf Bass (1987) and Naus et al (1986). A striking result of these evaluations is the very high arrest values. K_{Ia} well above $400 \text{ MPa}\sqrt{\text{m}}$ is observed in Fig 5.3. This observation motivated a study that takes into account rate-dependent plasticity. It can be suspected that some portion of the elastodynamically calculated K_I is due to combined viscous and plastic effects which are not connected only to the propagation of the crack-tip. Fig 5.5 shows the adopted viscoplastic constants of the Perzyna model compared with the experiments performed by Kanninen et al (1986 a).

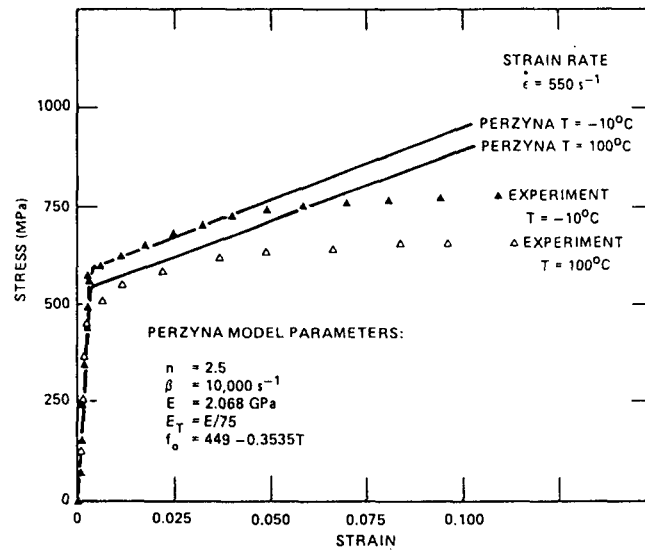


Fig 5.5. Comparison of adopted constants for the Perzyna model compared with measured stress-strain data for A533 B at a strain rate of 550 s^{-1} and at different temperatures.

Linear strain hardening is here assumed with a temperature-dependent yield stress f_0 . The result in terms of stress intensity factor as function of crack length is shown in Fig 5.6 and 5.7.

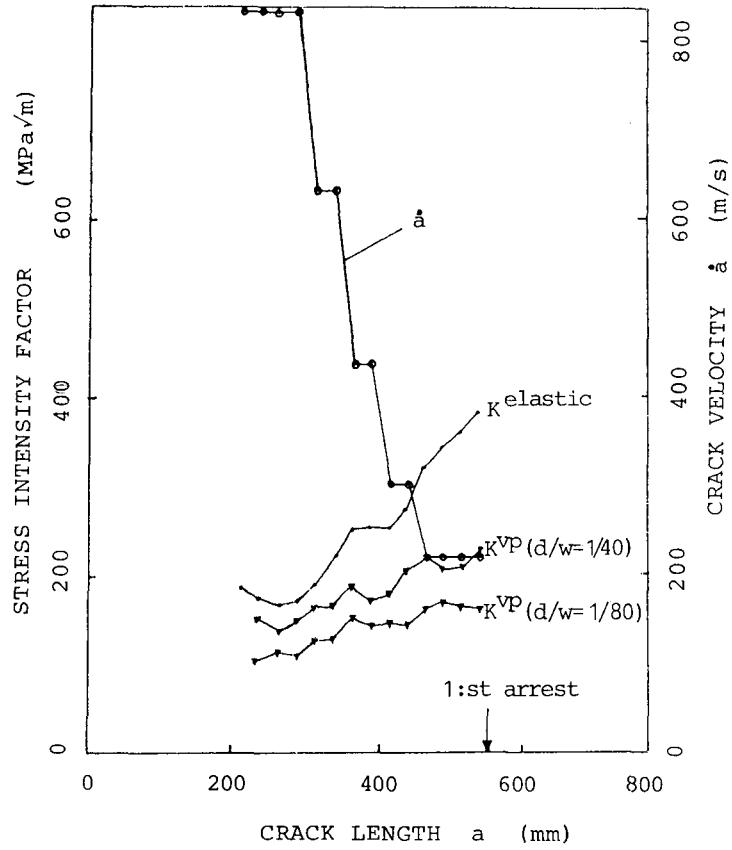


Fig 5.6 Stress intensity factor and crack velocity versus time for WP-1.2. Linear elastic and viscoplastic evaluations.

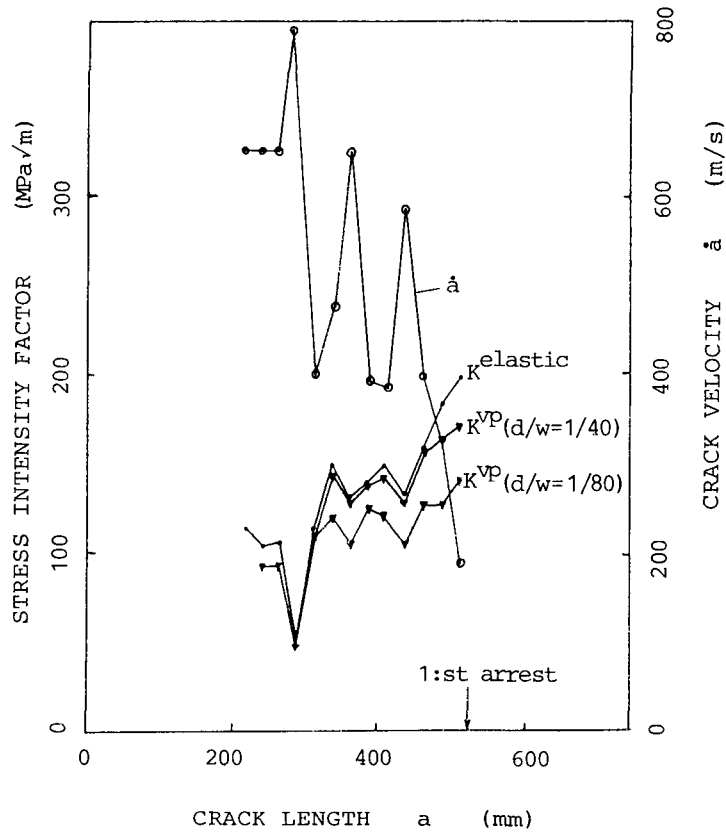


Fig 5.7 Stress intensity factor and crack velocity versus time for WP-1.5. Linear elastic and viscoplastic evaluations.

In Fig 5.6 and 5.7 a pseudo stress intensity factor is calculated in the viscoplastic case according to the procedure described in chapter 4. In these evaluations two sizes of the finite elements along the crack plane have been used. The following comments are made with reference to Fig 5.6 and 5.7.

- (i) A pronounced mesh-size dependence is obtained in the viscoplastic evaluations. Because of the asymptotic elastic behaviour for this choice of parameters in the Perzyna model, a convergence to a non-trivial result is expected for sufficiently small finite elements at the crack-tip. The study by Östlund (1988), indicates that a

size requirement of 10^{-1} - 10^{-5} of the size of the active plastic zone is needed for the small scale yielding case. This complicates the finite element modelling as well as the choice of a suitable fracture criterion. Apparently, a much smaller finite element size is needed along the crack plane in agreement with the conclusions by Bass et al (1988).

- (ii) For sufficiently small finite elements at the crack-tip, viscoplastic effects are always expected, even for a small scale yielding case. Still, an outer zone of K-dominance may exist, in which case the LEFM-theory should be sufficient.

Bearing the above comments in mind, the viscoplastic results in Fig 5.6 and 5.7 are only useful in a qualitative sense. The size of the active plastic zone ahead of the propagating crack-tip was quite large for wide-plate test 1.2, ranging from 20 mm to 125 mm prior to the first arrest. The corresponding data for WP-1.5 were 10 - 30 mm. This indicates that at least for WP-1.2, a conventional elastodynamic theory cannot be expected to give reliable result at crack arrest. The observed values of $\dot{\epsilon}_y$ at the nearest Gauss point were of the order of 50 - 200 s^{-1} for both tests. The numerically observed strain rates are of course very much dependent of the finite element size.

6. LARGE CCA-SPECIMEN TESTS

A series of eight instrumented experiments on the CCA-specimen have been conducted, four at the Norwegian Institute of Technology (SINTEF), two at The Technical Research Centre of Finland (VTT) and two at Risø National Laboratory in Denmark. The size of each specimen was approximately 400 x 400 x 100 mm.

The material is A533, B, Cl.1 steel in an austenitized, quenched and tempered condition. It was supplied from the program at ORNL, USA, which performed six wide-plate tests in 1985-86. After completion of a wide-plate test, the specimen was flame cut from the pull plates and the fracture surface was then cut away from each specimen half. Fig 6.1 shows a wide-plate specimen and the cutting plan for the CCA-specimens used in this investigation.

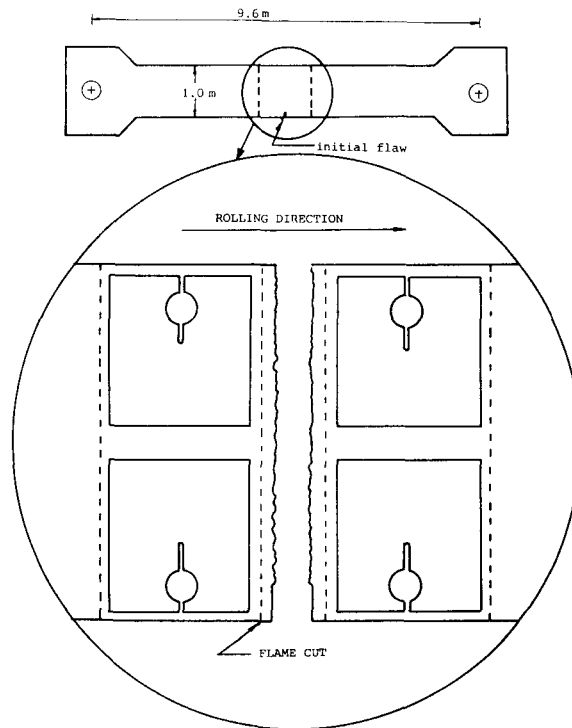


Fig 6.1 Cutting plan for compact test crack arrest specimen.

The used specimen type is a weld-embrittled side-wedge-loaded CT-specimen according to ASTM E 1221 (1988). The geometry and the processing of the embrittled weld are in accordance with the standard.

The material has the following chemical composition (wt %): 0.19 % C, 1.28 % Mn, 0.012 % P, 0.013 % S, 0.21 % Si, 0.64 % Ni and 0.55 % Mo. The plate was quenched and tempered as follows: 893 °C for 7.5 h, water quenched; 671 °C for 8.5 h, water quenched; 565 °C for 4 h, air cooled; 621 °C for 50 h and furnace cooled to 316 °C. An average grain size of ASTM 7 - 8 was measured for the material. Hardness was found to be 89 - 91 DPH (average) and did not vary through the thickness.

The average room-temperature tensile properties (longitudinal orientation) are ultimate tensile strength, 597 MPa; yield strength, 445 MPa; total elongation, 24 %; and reduction in area, 69 %. The RT_{NDT} was determined to be -23 °C, as measured by drop-weight/Charpy testing in the LT orientation, i.e. specimen parallel to the rolling direction and the notch transverse to the rolling direction. More information on mechanical properties is available in Naus et al (1987).

6.1 Quasistatic analysis

The following table specifies some geometrical dimensions and recorded values of the tests considered here

	T	a ₀	a _f	δ	B	B _N	ASTM K _{Ia}
SINTEF-1	-18°	118	274	δ _A =2.00	98	82	86.1
SINTEF-2	-16°	118	270	δ _A =1.80	98	82	77.5
VTT-2	-15°	120	276	δ _B =1.09	100	80	94.0
RISO-1	-16°	107	178	δ _D =1.15	99.5	80	89.6

T = test temperature, °C

a₀ = initial crack length, mm

a_f = arrested crack length, mm

δ_A, δ_B, δ_D = measured crack opening displacement (mm) at position A, B and D at initiation of crack growth, see Fig 6.3.

B, B_N = unnotched and notched thickness of specimen (mm)

K_{Ia} = Crack arrest toughness (MPa√m) according to the ASTM E 1221-88 standard.

The fracture surfaces of the SINTEF-specimens are shown in Fig 6.2.

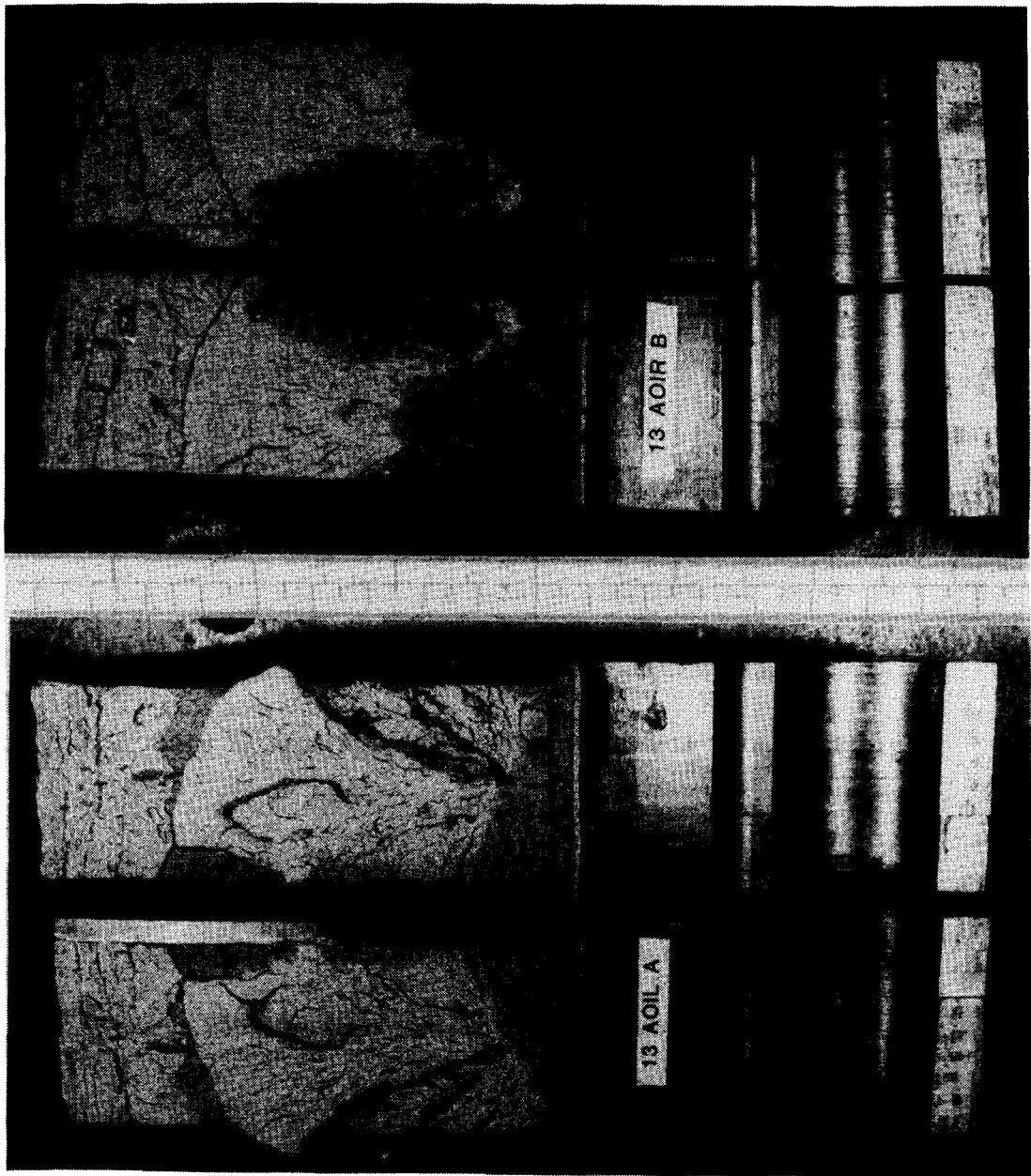


Fig 6.2 Fracture surfaces of two of the SINTEF specimens.

Fig 6.3 shows the finite element mesh used for both the quasistatic and the dynamic evaluations.

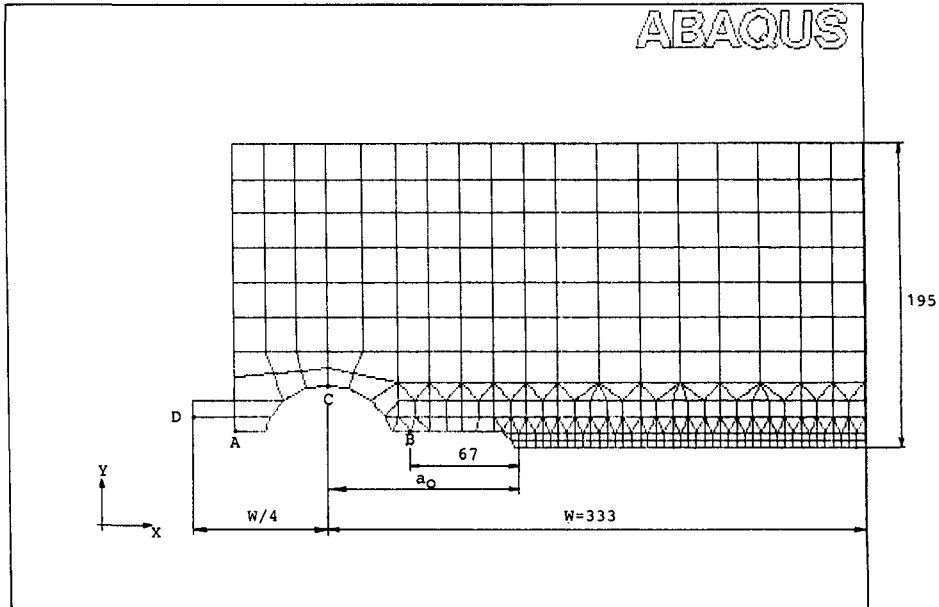


Fig 6.3 Finite element mesh showing upper half of CCA-specimen.

It consists of 374 4-node and 3-node elements with a total of 740 degrees of freedom. The single element at the front side of the specimen was placed there in order to obtain displacement values at a position $W/4$ from the load line as used in the ASTM-standard (1988). The element size along the crack plane is 5 x 5 mm.

The static stress intensity factor K_{I}^S was evaluated using two different methods and is shown as function of crack advance in Fig 6.4 for the SINTEF-2 experiment.

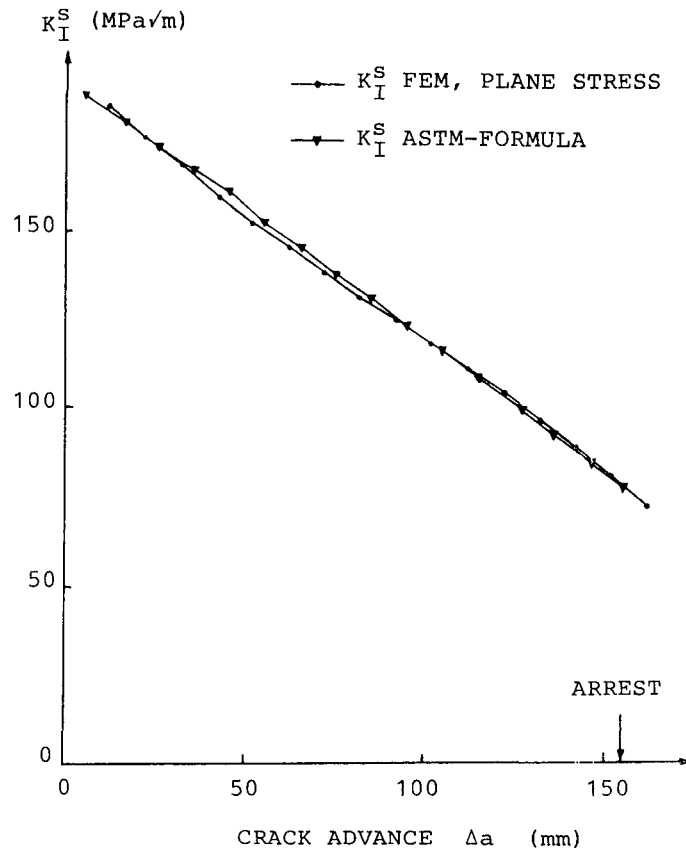


Fig. 6.4 Comparison of static stress intensity factors as functions of crack advance.

K_I^S , assuming global plane stress, is here determined by calculating the strain energy release rate for an incremental crack advance corresponding to a finite element distance along the crack plane. The displacement at the hole boundary (position C in Fig 6.3) was held constant in this calculation corresponding to the value at initiation of crack growth. Also shown in Fig 6.4 is K_I^S calculated by the method in the ASTM-Standard (1988),

$$K_I = \frac{E}{\sqrt{w}} \sqrt{\frac{B}{B_N}} v_1 f_1\left(\frac{a}{w}\right) \quad (6.1)$$

where f_1 is a compliance function given in the ASTM-standard (1988) and v_1 is the crack opening displacement at a distance $w/4$ behind the load line and was taken from the quasistatic finite element calculations at the respective crack arrest length. It is seen from Fig 6.4 that the finite element result agrees very well with the ASTM-formula (6.1).

It is also interesting to compare the quasistatic K_{Ia} -values from our four tests with the corresponding quasistatic evaluations according to the ASTM-standard (1988) obtained by ORNL on small specimens of the same material. This comparison is shown in Fig. 6.5.

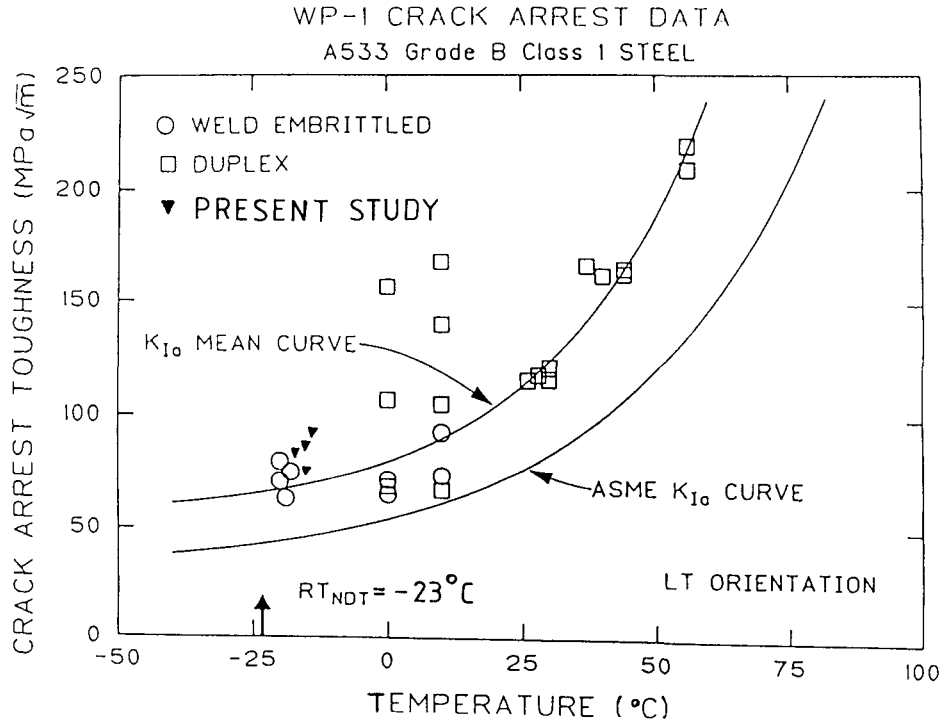


Fig 6.5 Comparison of quasistatic K_{Ia} in the present study with small specimen data obtained by ORNL.

It is observed that the K_{Ia} -values generated in this study compare well with the result from ORNL.

6.2 Dynamic analysis

Due to difficulties in the instrumentation technique, especially with signals from the strain gauges to detect the propagating crack front, only 3 experiments were judged to give reliable enough data to enable a complete dynamic analysis. The same finite element mesh as before and shown in Fig. 6.3 was used.

The instantaneous crack-tip position was determined by aid of strain gauges. The SINTEF-2 experiment is here chosen for closer study. In this experiment a set of 6 gauges were placed 58 mm above the intended crack plane. The spacing between the gauges were approximately 25 mm and the first gauge was located 55 mm from the initial crack-tip. Fig 6.6 - 6.8 show the recorded strain signals $\epsilon_y - \epsilon_x$ as function of time for the three first gauges.

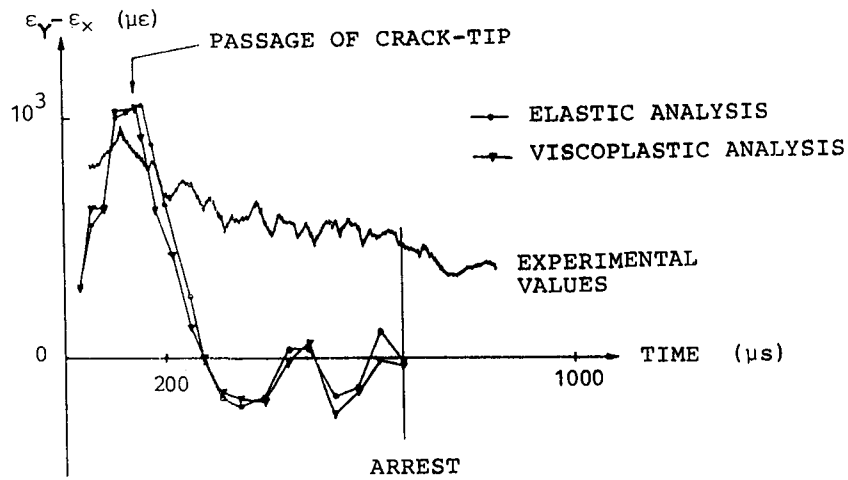


Fig 6.6 Strain $\epsilon_y - \epsilon_x$ as function of time for the first strain gauge. Experimental and numerical evaluations.

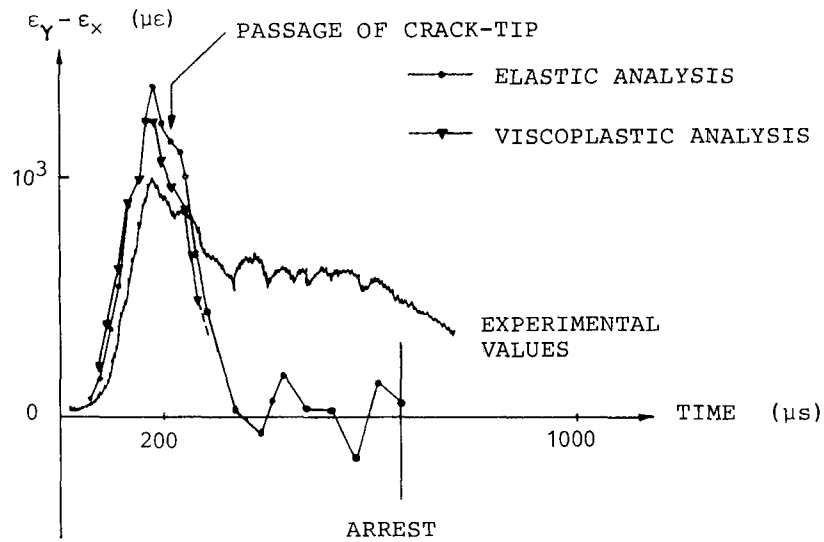


Fig 6.7 Strain $\epsilon_y - \epsilon_x$ as function of time for the second strain gauge. Experimental and numerical evaluations.

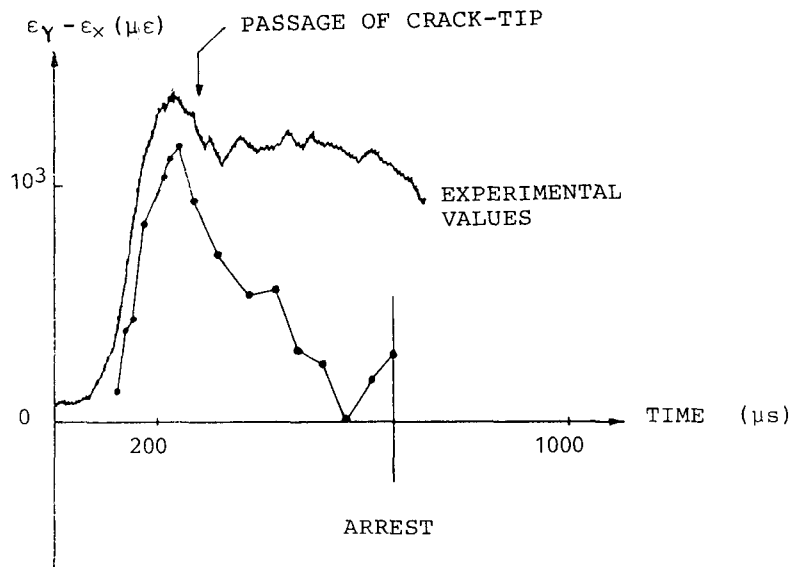


Fig 6.8 Strain $\epsilon_y - \epsilon_x$ as function of time for the third strain gauge. Experimental and numerical evaluations

The propagating crack-tip creates a singular strain field which can be traced by the strain gauges. By performing numerical finite element evaluations with different crack growth histories the computed strains can be matched against the experimental results. The numerically evaluated strain signals are also shown in Fig 6.6 - 6.8 for crack velocities that were considered to be the approximately true mean velocities between the gauge locations. Both the location and the width of the singular strain peak can be used to evaluate the crack velocity. It is seen that the peak of the strain signal is generally recorded some time before the actual passage of the crack tip right below the particular strain gauge. This is also what is theoretically expected, cf. Giannakopoulos (1988). As shown by Fig 6.6 - 6.8, at least the location of the numerically evaluated strain peaks seem to agree reasonably well with the experimental values. However, the experiments appear to give a quite high strain level also after the passage of the crack-tip. This behaviour was not reflected in the numerical evaluations, not even by including rate-dependent plasticity as shown by Fig 6.6 - 6.7.

This deviation between computed and recorded strains after the passage of the crack-tip, has also been found in some of the analyses performed by ORNL in the HSST-program of Naus et al (1988). The crack velocities evaluated from Fig 6.6 - 6.8 were 362 m/s and 311 m/s between the first three gauges.

By using the so evaluated crack growth histories, the dynamic stress intensity factor K_I^d as function of time was calculated. The result is shown in Fig. 6.9-6.11 for the three dynamically evaluated experiments. Also shown in the figures are the measured crack-tip position $a(t)$ from the strain gauge signals and the corresponding quasistatic stress intensity factor K_I^s .

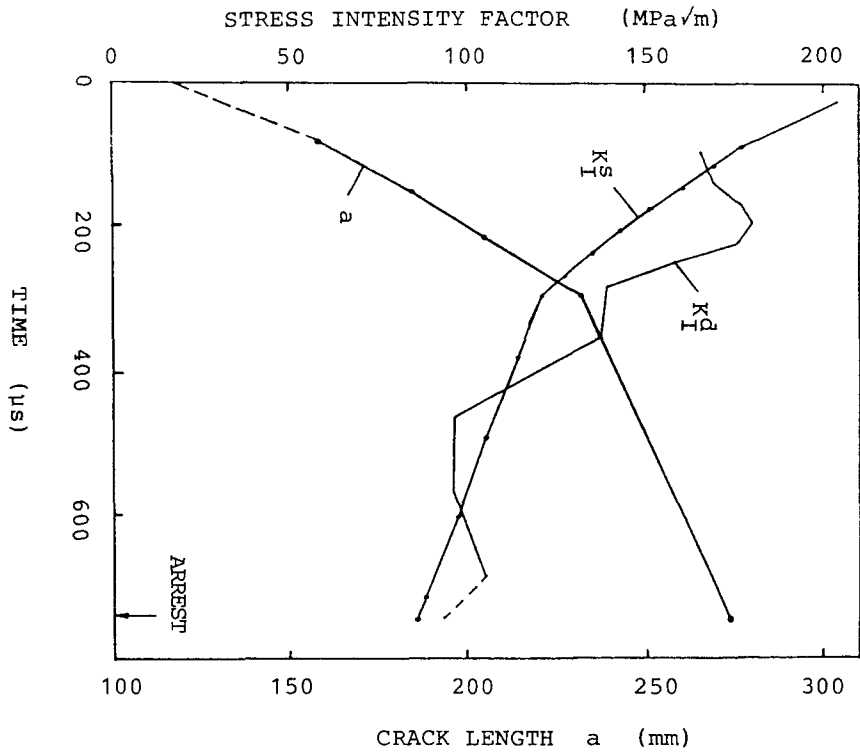


Fig 6.9 K_I , K_I^d and crack length as functions of time for experiment SINTEF-1.

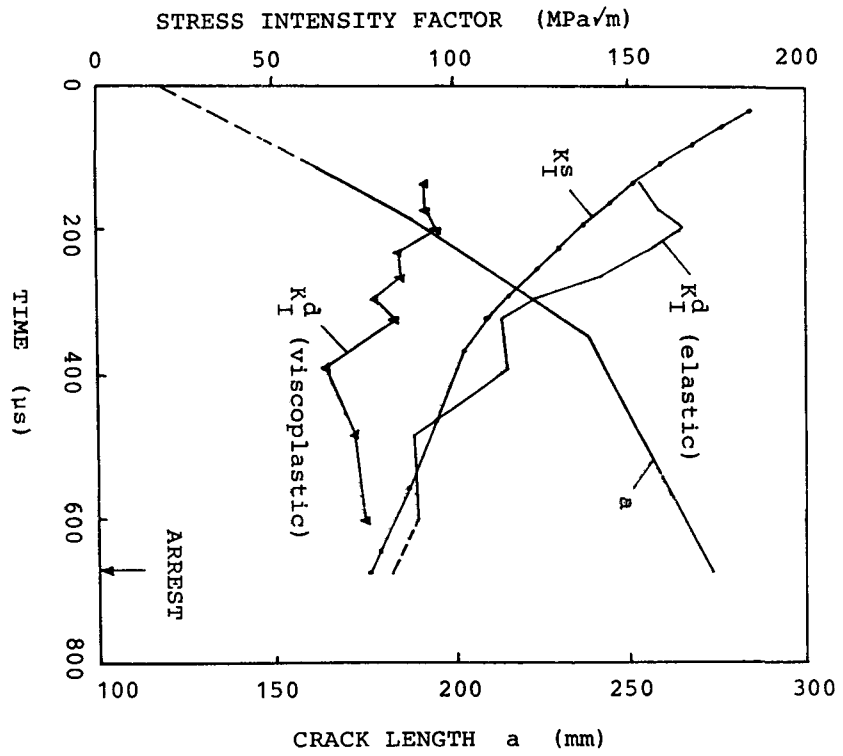


Fig 6.10 K_I^s , K_I^d , K_I^d and crack length as functions of time for experiment SINTEF-2.

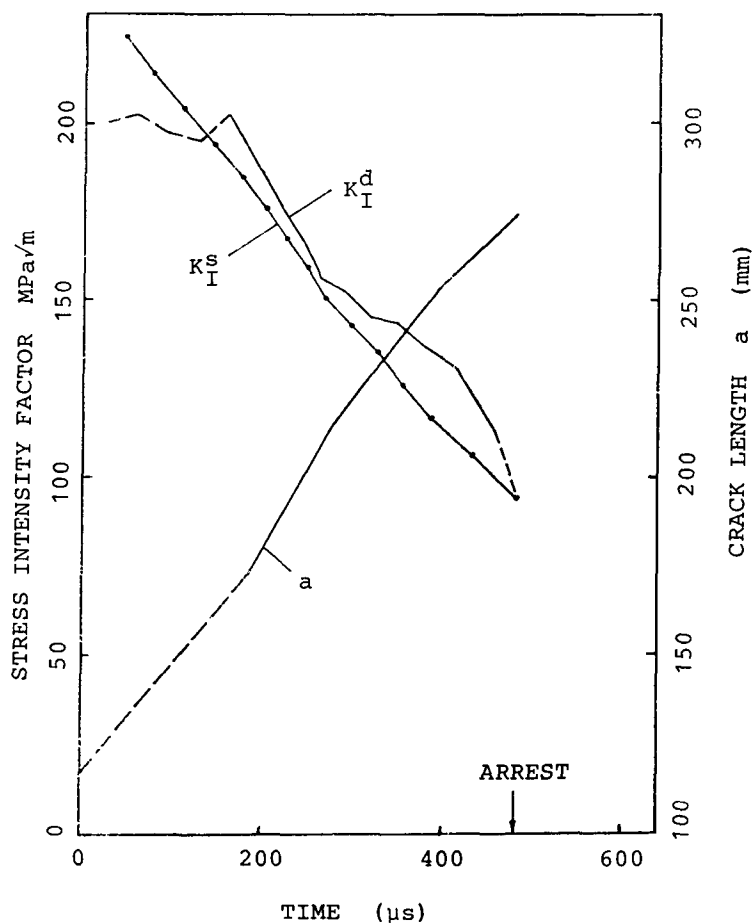


Fig 6.11 K_I^s , K_I^d and crack length as functions of time for experiment VTT-2.

Due to the scarce information of the rate of crack propagation during the first 50 mm of crack growth, a somewhat arbitrary constant crack velocity is assumed in this region in Fig 6.9 - 6.11. The K_I^d -values in this region should only be regarded in a qualitative sense. The arrest value K_{Ia} was determined by the calibrated nodal displacement method as described in chapter 4. It is observed that for all the considered

experiments the dynamic effects on $K_{I\dot{a}}$ seem to be fairly small, at least for the latter part of the propagation event. At crack arrest the difference between $K_{I\dot{a}}^s$ and $K_{I\dot{a}}^d$ is less than 10 percent in all three tests. This behaviour has also been confirmed by other investigators, see e.g. Khatri and Barker (1986).

The following table compares the dynamically evaluated $K_{I\dot{a}}$ with the quasistatic K_{Ia} from the ASTM-formula (6.1). Values given are in $\text{MPa}\sqrt{\text{m}}$.

Experiment	K_{Ia} (dyn)	K_{Ia} (static)
SINTEF-1	94.1	86.1
SINTEF-2	82.8	77.5
VTT-2	96.3	94.0

It is observed in this case that taking dynamic effects into account results in slightly higher crack arrest toughness values.

For one experiment, a viscoplastic evaluation was made. Here the viscoplastic parameters as shown in Fig 5.5 were used and the resulting pseudo stress intensity factor is shown in Fig 6.10. As expected, the introduction of viscoplasticity results in considerably lower values. As discussed in connection with the HSST-tests, a direct comparison with the elastodynamic K_I is not meaningful. However, it is interesting to note the size of the active plastic zone ahead of the propagating crack-tip, which varied from initially 15 mm to 2.5 mm prior to crack arrest for this experiment. Apparently, the plastic yielding was quite small when the crack arrested. The strain rate $\dot{\epsilon}_y$ at the nearest gauss point in front of the propagating crack-tip reached a maximum value of 400 s^{-1} with this resolution of the finite element mesh.

The computed displacements v and v_1 as function of time is shown in Fig 6.12 for one experiment.

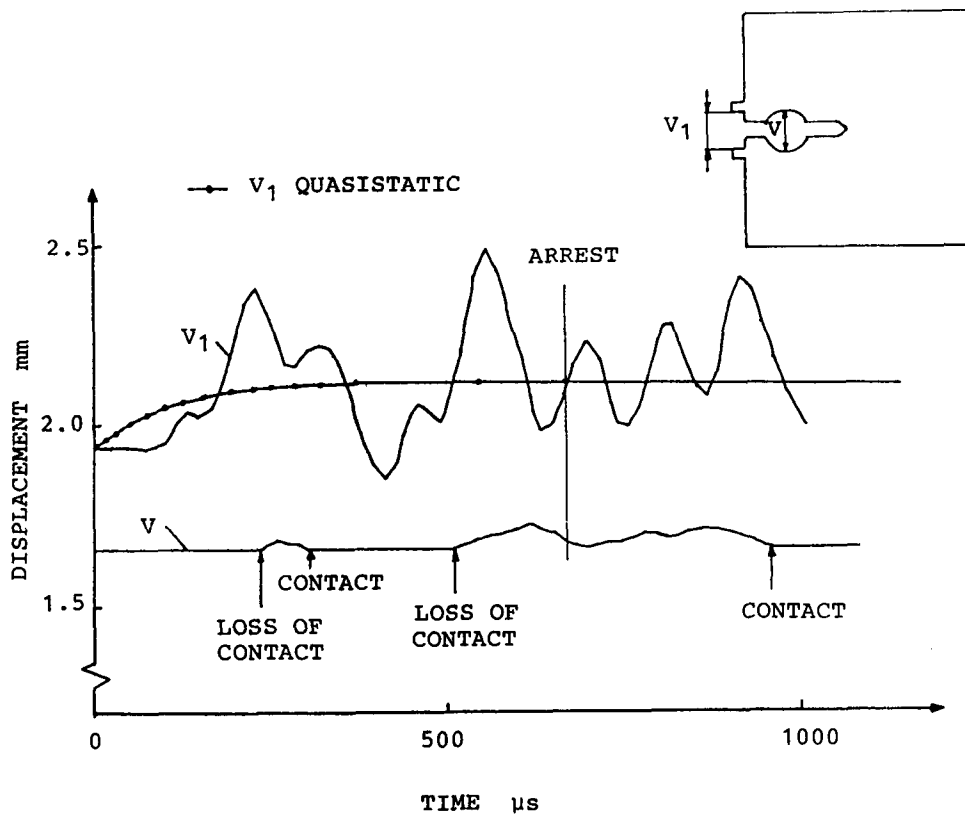


Fig 6.12 Evaluated displacement versus time for experiment SINTEF-2.

It is seen that the displacement v_1 is oscillating around the quasistatic value and that during a substantial time interval a loss of contact between the specimen and split pin is predicted. As discussed earlier this may have implications on evaluation of K_{Ia} according to the ASTM-formula (6.1).

From Fig 6.9 - 6.11, the crack propagation toughness K_{pc} as function of crack velocity can be deduced. The result is shown in Fig 6.13.

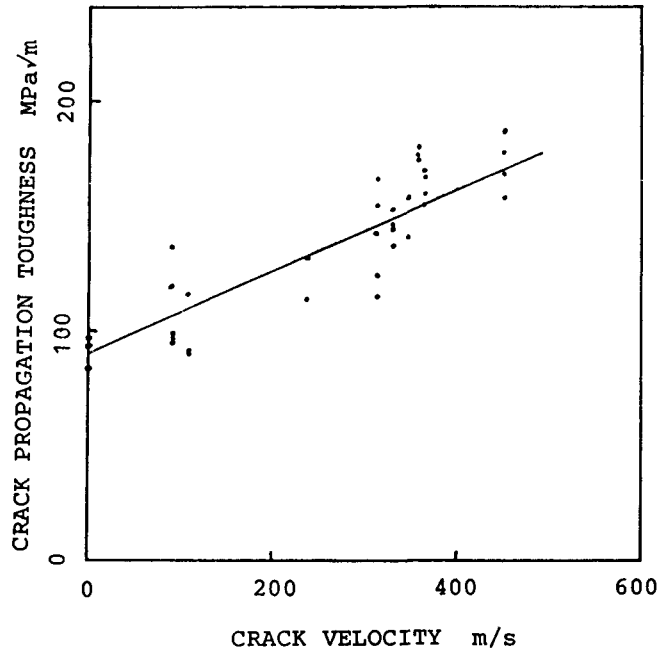


Fig 6.13 Crack propagation toughness K_{pC} as function of crack velocity for A533 B with $T - RT_{NDT} = 5$ to 8 °C.

The expected upward trend is reflected in Fig 6.13. Some portion of the observed scatter is probably due to the uncertainties in the experimental measurements. Providing this type of data is one of the main objectives with this study.

7. CONCLUSIONS

The following conclusions can be made from the NKA-program MAT 550.

- (1) An evaluation of K_{Ia} according to the ASTM standard E 1221 (1988) can be inaccurate if the specimen loses contact with the split pin at occurrence of crack arrest. This is a possibility that can not a priori be excluded. Analysis have shown that the contact can be lost during a crack event. The instantaneous displacement v at the split pin hole can, however, during loss of contact be measured at any point on the load line. Using the instantaneous displacement, instead of the displacement some time after crack arrest according to the ASTM standard, gives probably a better estimate in such a case.
- (2) A measurement of the displacement at any point on the load line during the experiment can also be used to verify the accuracy of a subsequent dynamic analysis.
- (3) An estimation of the crack velocity in the interior of a specimen may be obtained by using ultrasonic transducers, optical fibers or potential drop. All three methods need however to be further investigated to clarify their full potential.
- (4) The surface method for estimation of crack velocity based on strain gauges seems to work well also on large CCA-specimens if no crack tunneling effects occur.
- (5) The finite element program used for dynamic analysis in this investigation has been used for benchmark-analysis of the wide-plate experiments performed at NBS. The results agree well with results from ORNL which gives confidence in the reliability of the program.
- (6) Dynamic effects on the stress-intensity factor seem to be relatively small during a crack arrest test with the CCA-specimen.
- (7) The found crack propagation toughness values show an upward trend with increasing crack velocity as can be expected. The crack arrest toughness values agree well with the values obtained by ORNL.
- (8) Nonlinear material behaviour is likely to be important for A 533 B Cl. 1 steel at temperatures above the Charpy transition region.

ACKNOWLEDGEMENT

This project on crack propagation and arrest studies was financed by the Nordic Council of Ministers, The Swedish Nuclear Power Inspectorate, The Royal Norwegian Council for Science and Industrial Research, and The Minister for Trade and Industry in Finland. We want to express our gratitude for this support.

The support of free specimen material from The US Nuclear Regulatory Commission and Oak Ridge National Laboratory is greatly appreciated.

REFERENCES

- Aboudi, J. and Achenbach, J. D., (1983), *Int. J. of Frac.*, 21, pp 133 - 147.
- ASTM-standard E 1221, (1988), *Test Method for Determining the Plane-Strain Crack Arrest Fracture Toughness K_{Ia} of Ferritic Steels, 1988, Annual Book of ASTM Standards, American Society for Testing and Materials, Philadelphia, USA.*
- Ayres, D. J., Fabi, R. J., Peck, D. A. and Schoneberg, R. Y., (1986), "Test and analyses of crack arrest in reactor vessel materials in an increasing stress intensity field and increasing material toughness", *Combustion Engineering, Windsor, Connecticut, presented at the second review meeting on EPRI and NRC crack-arrest program, NBS, Gaithersburg. MD, USA.*
- Bass, B.R., (1987), *Third Annual Workshop on Dynamic Fracture and Crack Arrest Technology, NBS, Gaithersburg.*
- Bass, B.R., C.E. Pugh, (1988), Keeney-Walker, J. and Schwarz, C. W., *Int. J. Pres. Ves. and Piping* 31, pp 325 - 348.
- Brickstad, B. and Nilsson, F. (1980), *Numerical Methods in Fracture Mechanics* (edited by D. R. J. Owen and Luxmore, A. R.), pp 473 - 487.
- Brickstad, B., (1983 a), *Int. J. Fract.* 21, pp 177 - 194.
- Brickstad, B., (1983 b), *J. Mech. Phys. Solids*, 31, No. 4, pp 307 - 327.
- Bryan, R.H., Bass, B. R., Merkle, J. G., Pugh, C. E., Robinson, G. C. and Whitman, G. D. (1986), *Eng. Fract. Mech.*, 23, pp 81 - 97.
- Congleton, J. and Denton, B. K., (1977), *ASTM STP 627, G. T. Hahn and M. F. Kanninen, Eds., American Society for Testing and Materials, pp 336 - 358.*
- Dally, J. W. and Sandford, R. J., (1987), *Experimental Mechanics*, pp 381 - 388.
- deWit, R., Read, D., Low, S. R., McCloskey, D., Hicho, G. E., Harne, D. E., Smith, L. C. and Fields, R. J., (1985), *HSST Program Semiannual Progress Report April - September 1985, NUREG/CR-4219, Vol. 2, ORNL.*
- Douglas, A. S., (1982), "Dynamic Fracture toughness of ductile materials in antiplane shear", *Brown University, USA.*

- Fourney, W. L. and Chona, R. (1986), ASTM Round Robin on KIa-testing, presented at the second review meeting on EPRI and NRC crack-arrest programs, NBS, Gaithersburg, MD, USA.
- Freund, L. B. and Hutchinson, J. W., (1985), J. Mech. Phys. Solids, 33, pp 169 - 191.
- Freund, L. B., Hutchinson, J. W. and Lam, P. S., (1986), Eng. Fract. Mech., 23, No 1, pp 119 - 129.
- Giannakopoulos, A. E., (1988), TRITA-HFL-0098 ISSN 0281-1502, Report 98, Royal Inst. of Technology, Stockholm.
- Hui, C. Y. and Riedel, H., (1981), Int. J. of Fract., 17, p 409.
- Kanninen, M. F., Cardinal, J. W., Hudak, S. J., Polch, E. Z., Reed, K. W., Achenbach, J. D., Dexter, R. J. and Popelar, C. H., (1986 a), HSST Program Semiannual Progress Report April - September 1986, NUREG/CR-4219, Vol. 3, ORNL.
- Kanninen, M. F., Reed, K. W., Hudak, J. W., Polch, E., Z., Chan, K. S., Achenbach, J. D. and Popelar, C. H., (1986 b), "Development of a viscoplastic-dynamic fracture mechanics analysis model", presented at the second review meeting on EPRI and NRC crack-arrest programs, NBS, Gaithersburg, USA.
- Khatri, S. and Barker, D. B., (1986), ASTM STP 969, T.A. Cruse (editor).
- Lo, K. K., (1983), J. Mech. Phys. Solids, 31, pp 287 - 305.
- Lundberg, A., and Bryne, L. P., (1988), "Measurement of rapid crack growth with ultrasonic transducers", presented at the fourth annual HSST program workshop on dynamic fracture and crack arrest technology, NBS, Gaithersburgh, USA.
- Mc Cartney, L. N., (1982), Int. J. of Fract., 19, pp 99 - 113
- Melve, B., Hauge, M., Lundberg, A. and Thaulow, C., (1987), Int. J. of Fract., 34, pp R7 - R13.
- Naus, D. J., Keeney-Walker, J., Bass, B. R., Bolt, S. E., Fields, R. J., deWit, R. and Low, S. R., (1988), NUREG/CR-5330, ORNL/TM-11083.
- Naus, D. J., Pugh, C.E., Bass, B. R., Keeney-Walker, J., deWit, R. and Fields, R. J., (1986), "Summary of the fifth HSST wide-plate crack arrest test", Attachment to letter from C. E. Pugh to M. Vagins, NRC, February 7, 1986.

- Naus, D. J., Bass, B. R., Pugh, C. E., Nanstad, R. K., Merkle, J. G., Corwin, W. R. and Robinson, G. C., (1987), "Crack-Arrest behaviour in SEN wide plates of Quenched and tempered A533 grade B steel tested under nonisothermal conditions". NUREG/CR-4930, ORNL-6388.
- Nilsson, F., (1975), J. of Elasticity, Vol. 4, pp 73 - 75.
- Perzyna, P., (1966), Advances in Applied Mechanics, Vol. 9, p 243.
- Pugh, C. E., (1986 a), HSST Program Semiannual Progress Report, October 1985 - March 1986, NUREG/CR-4219, Vol. 1, ORNL.
- Pugh, C. E., (1986 b), "Program objectives and organization for the NRC/HSST-program", presented at the second review meeting on EPRI and NRC crack-arrest programs, NBS, Gaithersburgh, MD, USA.
- Rahka, K., (1980), J. of Testing and Evaluation, Vol. 8, No. 6, pp 318 - 323.
- Rahka, K., (1989), Eng. Fract. Mech., 32, No 3, pp 493 - 497.
- Rydholm, G., Fredriksson, B. and Nilsson, F., (1978), Numerical Methods in Fracture Mechanics (edited by Owen, R.R.J and Luxmoore, A.R.), p 660.
- Walsh, P. F., (1972), Technical Note, J. of the Engineering Mechanics Division, ASCE 98, pp 1611 - 1614.
- Östlund, S., (1988), TRITA-HFL-0095, ISSN 0281 - 1502, Report 95, Royal Inst. of Technology, Stockholm.

LIST OF PARTICIPANTS IN THE PROJECT

Denmark

Riso National Laboratory

Christian Debel

Finland

Technical Research Centre
of Finland (VTT)

Klaus Rahka
Jussi Solin

Norway

The Norwegian Institute of Technology
(SINTEF)

Mons Hauge
Arild Lundberg
Björn Melve
Christian Thaulow

Sweden

The Swedish Plant Inspectorate (SA)

Björn Brickstad
Lars Dahlberg
(project leader)

PUBLISHED REPORTS

- Brickstad, B. and Dahlberg, L., (1987), "Measurements and analysis of crack arrest experiments using the compact crack arrest specimen, SA/FOU-REPORT 87/06, The Swedish Plant Inspectorate, Stockholm.
- Brickstad, B. and Dahlberg, L., (1988), "Some aspects of performing dynamic measurements and analysis on the compact crack arrest specimen for A533 B steel", ASTM STP 969, T. A. Cruse, Ed., American Society for Testing and Materials, Philadelphia, USA, pp 532 - 546.
- Brickstad, B. and Dahlberg, L., (1989), "Measurement and evaluation of crack propagation and arrest experiments", Transactions of the 10th International Conference on Structural Mechanics in Reactor Technology, Volume G, pp. 119-124.
- Lundberg, A., and Bryne, L.P., (1988), "Measurement of rapid crack growth with ultrasonic transducers", Presented at the fourth annual HSST program workshop on dynamic fracture and crack arrest technology, National Bureau of Standards, Gaithersburgh, USA.
- Melve, B., Hauge, M., Lundberg, A. and Thaulow, C., (1987), Int. J. of Fract., 34, pp R7 - R 13.
- Rahka, K., (1989), Eng. Fract. Mech., 32, No 3, pp 493 - 497.

LIST OF PARTICIPANTS IN THE MAT 570 PROJECT

Finland

Technical Research Centre of Finland

Kari Törrönen
Rauno Rintamaa
Kim Wallin
Kari Ikonen
Heikki Keinänen
Heli Talja
Arja Saarenheimo
Klaus Rahka
Matti Sarkimo

Finnish Centre for Radiation and
Nuclear Safety

Rainer Rantala
Christer Ottosson

Neste Oy

Paavo Kuusela

Imatra Power Company

Ralf Ahlstrand
Tapani Kukkola

Industrial Power Company Ltd.

Erkki Pulkkinen

Helsinki Energy Board

Touko Ahonen

Technical Inspection Centre

Jarmo Kontro

Oy Huber Ab

Ari Juva

Sweden

Royal Institute of Technology

Fred Nilsson
Hans Öberg
Jonas Faleskog

Swedish Nuclear Power Inspectorate

Margareta Trolle

Denmark

Risø National Laboratory

Christian Debel

Jutland Technological Institute

Find Rotvel

Norway

Veritec

Stig Wästberg 1)

Veritas Research

Steven Slatcher
Finn Kirkemo

SINTEF

Mons Hauge
Morten Hval

1) Project leader